



# Biomechanical Analysis of Fixation Devices for Lumbar Interbody Fusion

Joana Maria Lemos Ferreira Real

Thesis to obtain the Master of Science Degree in  
Biomedical Engineering

Supervisor(s): Prof. Paulo Rui Alves Fernandes  
Prof. André Paulo Galvão de Castro

Examination Committee

Chairperson: Prof. Patrícia Margarida Piedade Figueiredo

Supervisor: Prof. André Paulo Galvão de Castro

Members of the Committee: Prof. Luís Alberto Gonçalves de Sousa  
Dr. Manuel José Tavares de Matos

October 2019



## ***Declaration***

*I declare that this document is an original work of my own authorship and that it fulfills all the requirements of the Code of Conduct and Good Practices of the Universidade de Lisboa.*



## *Preface*

*The work presented in this thesis was performed at the Department of Mechanical Engineering of Instituto Superior Técnico (Lisbon, Portugal), during the period February-October 2019, under the supervision of Prof. Paulo Fernandes and Prof. André Castro.*



## *Agradecimentos*

Em primeiro lugar gostaria de agradecer aos meus orientadores: os professores André Castro e Paulo Fernandes, pela ajuda que me deram ao longo destes meses. Um obrigado especial ao Prof. André pela paciência em todas as vezes em que começava a entrar em pânico por pensar que ia ter de refazer o modelo.

Um grande obrigado aos meus pais e à Milinha, pelo apoio e por me terem permitido ter as experiências que tive. Aos meus irmãos, João e Diana, por serem os melhores antídotos para o stress.

Ao Nikhil, por todas as vezes em que me ouviu pacientemente, me assegurou que ia tudo correr bem e me motivou a dar o meu melhor sempre.

Àqueles que biomédica me deu e que me ajudaram a manter a minha sanidade mental nestes cinco anos: Leonor, Diana, Mariana, Pedro, Cláudia, Marta e Rodrigo.

Um grande obrigado também àqueles que, mesmo não sendo da mesma faculdade, me apoiaram ao longo desta etapa e das anteriores também: Cati, Catarina, Rita, Daniela, Joana, Rute e Mariana.

Por último, gostaria de agradecer à Valentina por ter partilhado a “quest” da coluna, e também ao Rafael, ao Tiago, ao Gonçalo, à Mónica, à Joana e ao Alex pela ajuda e companhia dos últimos meses.



## *Abstract*

Disorders of the lumbar spine constitute a cause of disability. Different approaches to lumbar fusion have been developed throughout the years, in terms of the surgery procedure, the implants and the additional fixation. Although commonly used, fusion poses some risks, such as the degeneration of the adjacent segment. Finite Element models can be useful tools to increase the understanding of these problems.

The objective of this work was the simulation of the biomechanical response of the spine after an Oblique Lumbar Interbody Fusion procedure. This was achieved using an idealized model of the L3 to L5 spine, designed in Solidworks® and implemented in Abaqus®. It comprised the vertebrae, intervertebral discs and ligaments. The intact model, the instrumented one and both of them with disc properties altered to represent degeneration, were then loaded with a follower load of 100 N and a moment of 7.5 Nm to simulate extension, flexion, axial rotation and lateral bending. The range of motion, stress on the adjacent disc and on the instrumentation could then be evaluated.

The bilateral model performed better in terms of restricting the range of motion at the fusion segment and achieving lower Von Mises stress on the posterior fixation. However, studies with more complex models are required to assess the ability of the unilateral and cage only models to ensure adequate fusion. No difference was found in the stress on the adjacent disc for the different fixations, but stress increased after the instrumentation was applied, which may lead to degeneration.

Keywords: Lumbar spine, Oblique Lumbar Interbody Fusion, Finite Element model



## *Resumo*

As doenças da coluna lombar são uma causa de incapacidade e, nesse âmbito, foram desenvolvidas diferentes abordagens à fusão lombar ao longo dos anos, em termos do procedimento cirúrgico, dos implantes e da fixação adicional. Embora seja um procedimento geralmente utilizado, a fusão tem riscos que os modelos de elementos finitos podem ajudar a compreender melhor, como a degeneração do segmento adjacente.

O objetivo deste trabalho foi a simulação da resposta biomecânica da coluna após uma fusão intersomática lombar oblíqua, usando um modelo idealizado de L3 a L5, desenhado em Solidworks e implementado em Abaqus. O modelo era composto pelas vértebras, disco intervertebral e ligamentos. O modelo intacto, o instrumentado e ambos os casos com as propriedades do disco alteradas para simular degeneração foram postos sob uma *follower load* de 100 N e um momento de 7.5 Nm para simular extensão, flexão, torção e flexão lateral. A amplitude de movimentos e a tensão no disco adjacente e na instrumentação puderam então ser avaliados.

O modelo bilateral teve um melhor desempenho em termos da restrição da amplitude de movimentos no segmento fundido e da menor tensão de Von Mises na fixação posterior. No entanto, são necessários estudos com modelos mais complexos para avaliar a capacidade dos modelos unilaterais e do modelo só com a *cage* para atingir um nível de fusão adequado. Não foram encontradas diferenças na tensão no disco adjacente para as diferentes fixações, mas a tensão aumentou depois da introdução da instrumentação, o que poderá levar à degeneração.

Palavras-chave: Coluna lombar, Fusão Intersomática Lombar Oblíqua, Modelo de Elementos Finitos



# Contents

Declaration .....	i
Preface.....	iii
Agradecimientos .....	v
Abstract .....	vii
Resumo.....	ix
List of figures .....	xiii
List of tables .....	xv
List of acronyms.....	xvii
Nomenclature.....	xix
Introduction.....	1
1.1 Motivation and Contribution to the Surgical Practice .....	1
1.2 Objectives.....	2
1.3 Thesis Outline .....	2
Literature Review .....	3
2.1 Anatomy of the human spine.....	3
2.2 Spine diseases and instrumentation .....	5
2.3 Finite Element Models.....	9
Methodology .....	13
3.1 Intact model .....	13
3.2 Instrumented model.....	18
3.3 Simulation of degeneration.....	20
3.4 Results Presentation.....	21
Validation .....	23
4.1 Convergence study for the mesh .....	23
4.2 Selection of the ligament properties.....	24
4.3 Selection of the Follower Load .....	26
Results and Discussion .....	29
5.1 Range of Motion.....	29
5.1.1 Degenerated models .....	29
5.1.2 Instrumented models .....	31
5.1.3 Degenerated instrumented models .....	34
5.2 Stress .....	37
5.2.1 Adjacent disc .....	37

5.2.2 Instrumentation .....	43
5.3 Discussion Summary.....	45
5.4 Limitations.....	46
Conclusions and Future Work .....	47
References.....	49

## *List of figures*

### **Chapter 2**

Figure 2.1 Lateral view of a spinal unit, composed of 2 vertebrae and one IVD. Adapted from [10].	3
Figure 2.2 Upper (left) and lateral (right) view of a lumbar vertebra. 1 – vertebral body; 2 – pedicle; 3 – transverse process; 4 – spinous process; 5 – vertebral foramen; 6 – lamina; 7 – superior articular process; 8 – inferior articular process. Adapted from [11].	4
Figure 2.3 Sagittal section of the spine, showing five of the seven ligaments. Adapted from [13].	5
Figure 2.4 IVD, adapted from [12].	5
Figure 2.5 Different approaches to interbody fusion for five different procedures. The arrows indicate the path to access the disc space. Adapted from [17].	7
Figure 2.6 Representation of two possible interbody cages to use in the PLIF (left) and TLIF (right) procedures. Adapted from [23].	8
Figure 2.7 Two examples of devices used in total disc replacement: the Chatité III (left) and the Kineflex (right) [25].	8
Figure 2.8 Model by Belytschko et al., adapted from [28] (on the left) and one spinal segment, without the IVD, from the Breau et al. model, adapted from [29] (on the right).	10
Figure 2.9 Model of the lumbar spine developed by Chen et. al [7].	10
Figure 2.10 On the top, from left to right: moon-shaped cage placed in the middle, moon-shaped cage placed anteriorly and left diagonal cage. On the bottom, the instrumented model with bilateral posterior fixation (left) and unilateral posterior fixation (right). Adapted from [3].	11
Figure 2.11 Cage positions in the different procedures simulated. From left to right: OLIF, XLIF, TLIF with a banana-shaped cage and TLIF with a straight cage. Adapted from [16].	12

### **Chapter 3**

Figure 3.1 Posterior (left), lateral (middle) and anterior (right) view of the model of one lumbar vertebra in Solidworks®. The vertebral body was created in [8] and the posterior elements were added in the present work.	13
Figure 3.2 Lateral view of the complete model L3 to L5 (left) and superior view of one IVD (right), both created in Solidworks®. 1 – vertebral body; 2 – IVD; 3 – superior articular process; 4 – pedicle; 5 – transverse process; 6 – spinous process; 7 – inferior articular process; 8 – AF; 9 – NP.	16
Figure 3.3 Abaqus® model of the vertebrae L3 to L5, showing the referential in reference to which the different loads were applied.	18

Figure 3.4 Superior-lateral (upper left) and superior (upper right) views of the cage. Model of the screw (bottom left) and bar (bottom right) used in the posterior fixation. ....	18
---	----

Figure 3.5 Anterior (left) and lateral right (right) view of the L3 to L5 model without posterior fixation and with the cage inserted at the L4-L5 level. ....	19
--	----

Figure 3.6 Posterior view of the unilateral left (left), bilateral (middle) and unilateral right (right) models. ....	20
---	----

## Chapter 4

Figure 4.1 Von Mises stress on a node on the interface between the L3 vertebra and the upper IVD, as a function of the number of elements. ....	24
---	----

## Chapter 5

Figure 5.1 Maximum principal stress in the L3-L4 healthy (left) and mildly degenerated (right) disc when the bilateral model is subjected to E. ....	38
--	----

Figure 5.2 Maximum principal stress on the L3-L4 disc of the non-instrumented healthy model (left) and of the cage only model with upper disc healthy (right), when subjected to Flex. ....	38
---	----

Figure 5.3 Maximum principal stress in the L3-L4 healthy (left) and mildly degenerated (right) disc when the bilateral model is subjected to Flex. ....	39
---	----

Figure 5.4 Maximum principal stress in the L3-L4 healthy (left) and mildly degenerated (right) disc when the bilateral model is subjected to left AR. ....	40
--	----

Figure 5.5 Maximum principal stress on the L3-L4 disc of the unilateral left model, when subjected to left LB (left) and right LB (right). ....	40
---	----

Figure 5.6 Maximum principal stress in the L3-L4 healthy (left) and mildly degenerated (right) disc when the bilateral model is subjected to right LB. ....	41
---	----

## *List of tables*

### **Chapter 3**

Table 3.1 Dimensions of the model. ....	14
Table 3.2 Constitutive models and parameters used in Abaqus®. All values were taken from [8]. ....	16
Table 3.3 Number of ligaments of each type and description of structures they connected in the model. ....	17
Table 3.4 Dimensions of the cage and posterior fixation devices and material properties given to the FE model. ....	19
Table 3.5 Values found in [38] for the mildly and moderately degenerated NP (Young's Modulus and Poisson's ratio) and AF (C10 parameter and Poisson's ratio). ....	21
Table 3.6 Coefficients used in the present work's material formulations of the AF and NP for the healthy, mildly degenerated and moderately degenerated cases. ....	21

### **Chapter 4**

Table 4.1 Range of Young's modulus [30] and cross-sectional areas [41] found in the literature. The values obtained dividing the cross-sectional areas by the number of each type of ligaments in the model of the present study are also presented. ....	25
Table 4.2 Values of the ROM in degrees: minimum, median and maximum found in the literature [11]. In blue, the values obtained in the simulation. ....	25
Table 4.3 Ligament properties after validation. ....	26
Table 4.4 ROM, in degrees, obtained for the model subjected to the moment and FL indicated, in E, Flex, AR and LB. ....	27

### **Chapter 5**

Table 5.1 Combinations of IVD states considered in the analysis. ....	29
Table 5.2 ROM, in degrees, obtained for the four movements for different combinations of degeneration states of the discs. The values in gray are the percentage changes relative to the healthy case, (1). ....	30
Table 5.3 Segmental ROM of the L3-L4 spinal unit, in degrees, obtained for the four movements, with the upper disc healthy and the three possible bottom disc states. The values in gray are the percentage changes relative to the healthy case, (1). ....	30
Table 5.4 Segmental ROM of the L4-L5 spinal unit, in degrees, obtained for the four movements, with the upper disc healthy and the three possible states of the bottom disc. The values in gray are the percentage changes relative to the healthy case, (1). ....	31

Table 5.5 ROM, in degrees, of the healthy model and the four instrumented ones. The values in gray are the percentage changes relative to the healthy case.....	32
Table 5.6 ROM of the L3-L4 segment, in degrees, for the healthy and instrumented cases. The values in gray are the percentage changes relative to the healthy case.....	32
Table 5.7 ROM of the L4-L5 segment, in degrees, for the healthy and instrumented cases. The values in gray are the percentage changes relative to the healthy case.....	33
Table 5.8 ROM, in degrees, of the instrumented models with the L3-L4 mildly degenerated, for all the motions. The values in gray are the percentage changes relative to the instrumented models with healthy upper IVD.....	35
Table 5.9 ROM, in degrees, for degeneration case (4) and the cage only model with the adjacent disc healthy, for all motions. The values in gray are the percentage changes relative to degeneration case (4). .....	35
Table 5.10 ROM, in degrees, for degeneration case (5) and the cage only model with the adjacent disc mildly degenerated, for all motions. The values in gray are the percentage changes relative to degeneration case (5).....	35
Table 5.11 ROM of the L3-L4 segment, in degrees, of the instrumented models with the adjacent disc mildly degenerated. The values in gray represent the percentage changes relative to the instrumented models with the adjacent disc healthy. ....	36
Table 5.12 ROM of the L4-L5 segment, in degrees, of the instrumented models with the adjacent disc mildly degenerated. The values in gray represent the percentage changes relative to the instrumented models with the adjacent disc healthy.....	36
Table 5.13 Maximum pressure acting on the NP, in MPa, for the non-instrumented healthy model and instrumented with bilateral fixation having an adjacent disc healthy or mildly degenerated. The values in gray are the percentage changes relative to the first case.....	41
Table 5.14 Maximum Von Mises stress, in MPa, acting on the cage for the various instrumented models. The values in gray are the percentage changes relative to the cage only model. ....	43
Table 5.15 Maximum Von Mises stress, in MPa, on the posterior instrumentation for all the types of constructs. ....	43
Table 5.16 Maximum Von Mises stress, in MPa, on the posterior instrumentation for all the types of constructs with the adjacent disc mildly degenerated. ....	44

## *List of acronyms*

<b>AF</b>	annulus fibrosus
<b>ALIF</b>	anterior lumbar interbody fusion
<b>ALL</b>	anterior longitudinal ligament
<b>AR</b>	axial rotation
<b>CL</b>	capsular ligament
<b>DDD</b>	degenerative disc disease
<b>E</b>	extension
<b>FE</b>	finite element
<b>FL</b>	follower load
<b>Flex</b>	flexion
<b>ISL</b>	interspinous ligament
<b>ITL</b>	intertransverse ligament
<b>IVD</b>	intervertebral disc
<b>LB</b>	lateral bending
<b>LF</b>	ligamentum flavum
<b>NP</b>	nucleus pulposus
<b>OLIF</b>	oblique lumbar interbody fusion
<b>PLIF</b>	posterior lumbar interbody fusion
<b>PLL</b>	posterior longitudinal ligament
<b>ROM</b>	range of motion
<b>SSL</b>	supraspinous ligament
<b>TLIF</b>	transforaminal lumbar interbody fusion
<b>XLIF</b>	extreme lateral interbody fusion



## *Nomenclature*

$c_{10}$	
D	
$k_1$	Material parameters for the Holzapfel model
$k_2$	
kappa	
U	Strain energy per unit of reference volume
$\bar{I}_1, \bar{I}_2$	Deviatoric strain invariants
$J^{el}$	Elastic volume ratio
$c_{10}$	
$c_{01}$	Material parameters for the Mooney-Rivlin model
$D_1$	
E	
k	bulk modulus
$\nu$	Poisson's ration



# ***Chapter 1***

## **Introduction**

This chapter gives the motivation of this work, the way it contributes to the surgical practice, its goals and its outline.

### **1.1 Motivation and Contribution to the Surgical Practice**

Lumbar spine conditions related to degeneration are a serious source of disability worldwide. Degenerative diseases include degenerative disc disease (DDD), spondylolisthesis (wherein a vertebra suffers a displacement relative to the adjacent one) and stenosis (narrowing of the spinal canal). They are also correlated with a variety of symptoms, from lower extremity pain to low back pain, that in the most severe cases can greatly impact people's quality of life [1].

In order to better diagnose and treat spinal instability, as well as to create implants and models to design surgery, it is of utmost relevance to understand the biomechanics of the spine. Since in-vitro and in-vivo studies have some inherent limitations, computational models are useful tools in the investigation of these issues [2].

Moreover, Finite Element (FE) studies allow one to compare different interventions, and to solve related questions, for example, whether bilateral posterior fixation is paramount for stabilizing the spinal segment, or if unilateral pedicle screws can provide sufficient fixation for bone fusion to occur. On the one hand, bilateral fixation leads to a greater Range Of Motion (ROM) restriction and smaller stresses on the Annulus Fibrosus (AF) and instrumentation, as shown in [3] for Transforaminal Lumbar Interbody Fusion (TLIF). In fact, in a study where radiographic results after TLIF were measured, unilateral fixation caused a greater loss of Intervertebral Disc (IVD) height and segmental lordosis at follow-up of 1 or 3 months [4]. On the other hand, [5] showed that unilateral fixation caused stability similar to the bilateral one in TLIF, after achieving bone graft fusion. Furthermore, in a meta-analysis of Posterior Lumbar Interbody Fusion (PLIF) studies [6], not only were the two similar in terms of fusion rate, Japanese Orthopedic Association score and Visual Analogue Scale score, but the unilateral model provided smaller blood loss and operative time, shorter hospital stay and better Oswestry Disability Index score. Furthermore, unilateral fixation was considered as possibly able to prevent stress-shielding induced osteopenia in [4].

Another aspect that has been greatly discussed in the literature is how fusion changes the stress distribution, which in turn leads to degeneration of the adjacent segment [7]. FE models make it possible to test different degeneration stages and to study the effect of progressive degeneration.

The present work may aid surgical practice since it allows the test of different types of fixation, thus either supporting unilateral fixation and its inherent clinical advantages or securing the bilateral fixation role as the most efficient in facilitating fusion. It also provides a way to predict how the adjacent segment will be affected and to compare the situation where the fusion takes place next to a healthy disc or one that is already degenerated.

## **1.2 Objectives**

The goal of this work was, firstly, the simulation of the biomechanical response of the spine in the case of an Oblique Lumbar Interbody Fusion (OLIF) procedure, wherein only the cage is inserted or when it is aided by unilateral or bilateral posterior fixation, so the best approach could be inferred, considering the mechanical behavior and the surgery requirements of each one. Degeneration could also be simulated to understand its effect on the spine biomechanics and the difference between the behavior of the segments when the instrumentation was implanted with an adjacent healthy or degenerated disc.

To achieve this, an idealized CAD model of two vertebral segments was developed and validated. It comprised the spine from the third to the fifth lumbar vertebrae, L3 to L5, wherein each vertebra resulted from the addition of the vertebral arch to the vertebral body created in previous work [8]. The cage and devices used for posterior fixation were designed following the product specifications of the Medtronic's product [9].

## **1.3 Thesis Outline**

Chapter 2, the Literature Review, provides an introduction to the anatomy of the spine and the constitutive parts of the vertebra and of the IVD. It also gives an overview of the progress that has been made, not only in terms of interventions and instrumentation, but also in the development of FE models.

In Chapter 3, the Methodology for the construction of the model and the instrumentation in Solidworks<sup>®</sup> is described, as well as the steps taken in Abaqus<sup>®</sup> to create the final model and simulate the different loading situations and degeneration.

Chapter 4, Validation, introduces some of the tests undergone to choose certain aspects of the model, namely the size of the mesh, the properties of the ligaments and the Follower Load (FL) applied.

The 5<sup>th</sup> Chapter, Results and Discussion, contains the results obtained in the various simulations made, along with the comparison with the literature and respective discussion. It ends with a description of the limitations of this work.

Lastly, Chapter 6 contains the conclusions of the thesis and what should be done in the future, regarding the construction of more complex models to better understand these issues.

# ***Chapter 2***

## **Literature Review**

This chapter presents an overview of the spine anatomy and the options for the treatment of lumbar spine conditions. The last section presents a summary of the history of the development of the FE models of the spine.

### **2.1 Anatomy of the human spine**

The vertebral column has the purpose of encircling the spinal cord, guaranteeing its protection as well as that of the spinal nerves; supporting the head and serving as a connection point for the ribs, pelvic girdle and back muscles [10], [11].

The spine has cervical, thoracic and lumbar vertebrae, plus the sacrum and the coccyx. From the second cervical vertebra to the last lumbar one there is an IVD between each pair of vertebrae. Every pair and the disc in between constitute a spinal unit, as seen in Figure 2.1.

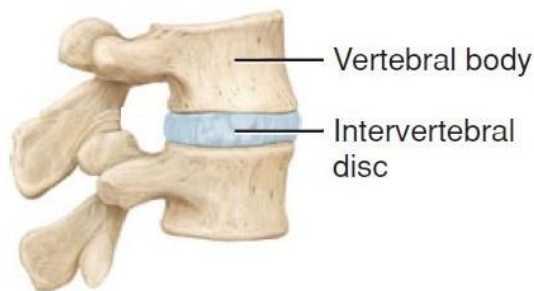


Figure 2.1 Lateral view of a spinal unit, composed of 2 vertebrae and one IVD. Adapted from [10].

Each vertebra has a disc-shaped body on its anterior part, the vertebral body. Its composition is mainly trabecular bone, enveloped by a cortical bone layer. As can be seen in Figure 2.2, the posterior part consists of the vertebral arch, encompassing the pedicles and the laminae. The two laminae fuse posteriorly, just before the spinous process. Between the body and the vertebral arch, there is a hole called vertebral foramen. When considering the vertebrae on top of each other, the aligned foramina form the vertebral cavity, through which the spinal cord runs. From the sides of the vertebral arch, where

the lamina and the pedicles of each side meet, a transverse process arises. Both of these and the spinous process, will be attachment points for the muscles and ligaments. There are four other articular processes: two superior ones, to articulate with the vertebra above, and two inferior ones, to articulate with the vertebra below. The surfaces where the processes meet are covered by hyaline cartilage [11].

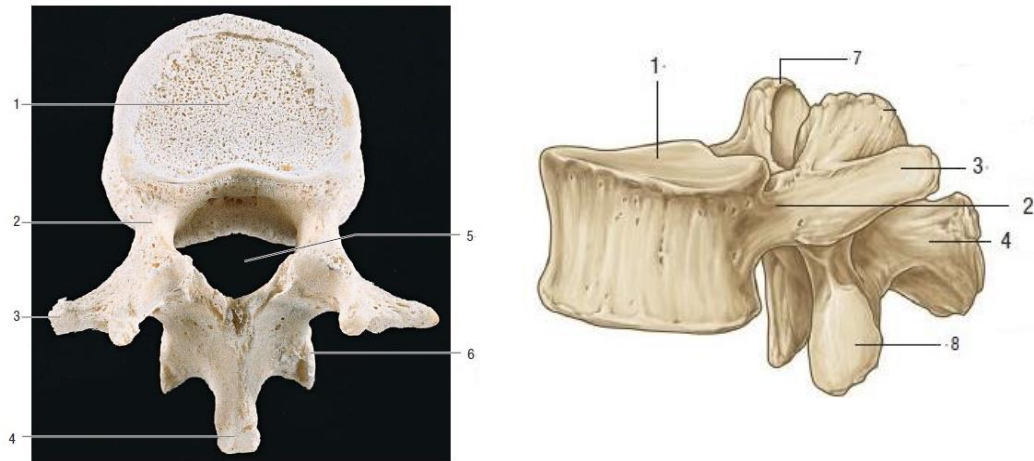


Figure 2.2 Upper (left) and lateral (right) view of a lumbar vertebra. 1 – vertebral body; 2 – pedicle; 3 – transverse process; 4 – spinous process; 5 – vertebral foramen; 6 – lamina; 7 – superior articular process; 8 – inferior articular process. Adapted from [11].

The movement of the vertebrae is restricted by seven types of ligaments, as listed below [11]. Among them, the first five connect the neural arch and the processes and the last two connect the vertebral bodies of adjacent vertebrae. Figure 2.3 shows a sagittal section of the spine with its ligaments, except for the intertransverse and capsular ones.

- Ligamentum flavum (LF): connects the internal surface of the laminae.
- Intertransverse ligaments (ITL): responsible for connecting the transverse processes.
- Interspinous ligaments (ISL): associate the spinous processes.
- Supraspinous ligaments (SSL): bind the peaks of the spinous processes.
- Capsular ligaments (CL): join the articular facet joints of adjacent vertebrae.
- Anterior longitudinal ligament (ALL): connect the anterior surface of adjacent vertebral bodies.
- Posterior longitudinal ligaments (PLL): attach the posterior surface of adjacent vertebral bodies.

An IVD distributes the pressure and allows its transmission to the adjacent vertebrae. It has approximately 4 cm of diameter and a thickness of 7 to 10 mm. In the lumbar region, its anterior part is thicker than the posterior one.

Each disc, as shown in Figure 2.4, is composed of the Nucleus Pulposus (NP) and the ring it is encircled by, the AF. The NP consists of collagen fibers and radial elastin fibers, all of them in a hydrated gel with a proteoglycan, aggrecan, in its composition. It has a higher water and proteoglycan content than the AF. The AF is a ring of fibrous cartilage with 15 to 25 rings or lamellae of parallel collagen fibers that make an angle of 60° to the right or to the left of the vertical axis (or 30° to the transverse plane) in

alternating lamellae. Between the various oriented layers, there are elastin fibers. The disc is in contact above and below with layers of hyaline cartilage, the endplates [11], [12].

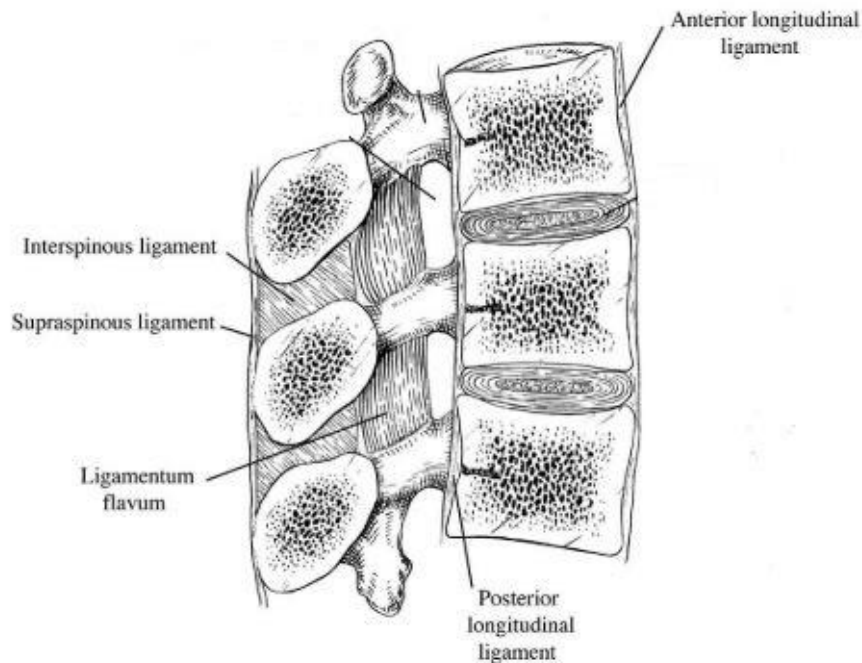


Figure 2.3 Sagittal section of the spine, showing five of the seven ligaments. Adapted from [13].

According to Gray [11], Flexion (Flex) is a movement forward, in which the ALL relaxes and the PLL, LF, ISL, and SSL are under tension. Extension (E) is the opposite motion: it is limited by the ALL and by the spinous processes getting closer to one another. In Lateral Bending (LB) one of the sides of the IVD is compressed and the movement is limited by the ligaments around. Axial Rotation (AR) occurs through the twisting of the IVD.

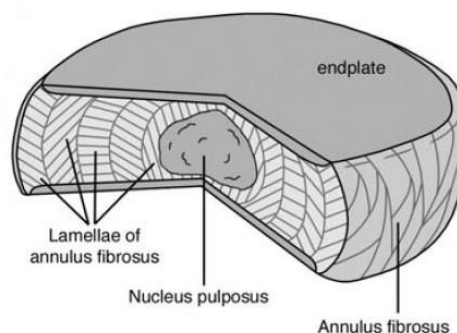


Figure 2.4 IVD, adapted from [12].

## 2.2 Spine diseases and instrumentation

One option for the treatment of low back pain is spinal fusion or arthrodesis [14], wherein two or more adjacent vertebrae are fused together, using an autograft (from the patient's iliac crest), an allograft

(from another individual), or other alternatives using demineralized bone matrix, ceramics, and bone morphogenic protein [15]. There are different fusion techniques, that approach the disc undergoing fusion through different channels, as presented in Figure 2.5. Furthermore, it can be supplemented with posterior pedicle screw fixation unilateral or bilaterally.

In **Posterolateral Fusion** an autograft is applied between the transverse processes [14]. However, compared to this technique, the lumbar interbody fusion procedures grant greater support in the anterior column and allow a bigger lordosis [16].

**Posterior Lumbar Interbody Fusion (PLIF)** was first introduced in 1944 by Briggs and Milligan. Since then, new options for the interbody implant have been developed, as well as pedicle screw fixators. The access to the IVD is done through the back and a laminectomy may be executed. Because of it being performed through the spinal canal, there is a risk of nerve root injury. This technique can be performed in cases of DDD, segmental instability, disc herniation, stenosis and pseudoarthrosis [17].

In 1982, Harms and Rolinger described a new posterior technique, **Transforaminal Lumbar Interbody Fusion (TLIF)**, in which the cage is inserted unilaterally through the intervertebral foramen. The procedure is done through the back and can be minimally invasive. The facet joints on the side of the intervention have to be removed, so the disc can be accessed and partially removed, and the cage can be inserted. Similarly to PLIF, pedicle screws can be used to help stabilize the segment. Although it avoids the spinal canal, there is still the risk of paraspinal muscle injury. Among its indications are DDD, disc prolapse, disc herniation, pseudoarthrosis and symptomatic spondylosis [14], [17].

An anterior approach, **Anterior Lumbar Interbody Fusion (ALIF)**, is also an option in the treatment of DDD, as well as of discogenic disease and revision of unsuccessful posterior fusion. When compared with posterolateral fusion, it has the advantage of reestablishing disc height, promoting load transmission and having lower operating time. However, since the aorta and vena cava have to be moved aside to access the spine, there is a risk of vascular lesions [14], [17].

Lateral approaches have the advantages of preserving the posterior column, having a shorter operative time and recovery period and producing a better decompression of the foramen and central canal [16]. Both the procedures presented below can be performed for all degenerative indications and amendment of sagittal and coronal deformities, such as lumbar degenerative scoliosis with laterolisthesis. Conversely, they are not suited for severe central canal stenosis and high-grade spondylolisthesis [17].

In **Extreme Lateral Interbody Fusion (XLIF)** an incision is made laterally, allowing the removal of the damaged IVD and its replacement with the cage. It has the advantage of avoiding major back muscles [14].

First outlined in 1977, the **Oblique Lumbar Interbody Fusion (OLIF)**, is similar to XLIF, although the incision used to insert the cage is done more anteriorly [17]. OLIF is the procedure that will be simulated in the present work.

XLIF is not advisable for the L5-S1 level because of the presence of the iliac crest, while OLIF can be used for all levels of L1-S1. Moreover the latter presents a smaller chance of lumbar plexus and psoas injury since the dissection is done anterior to the psoas [17].

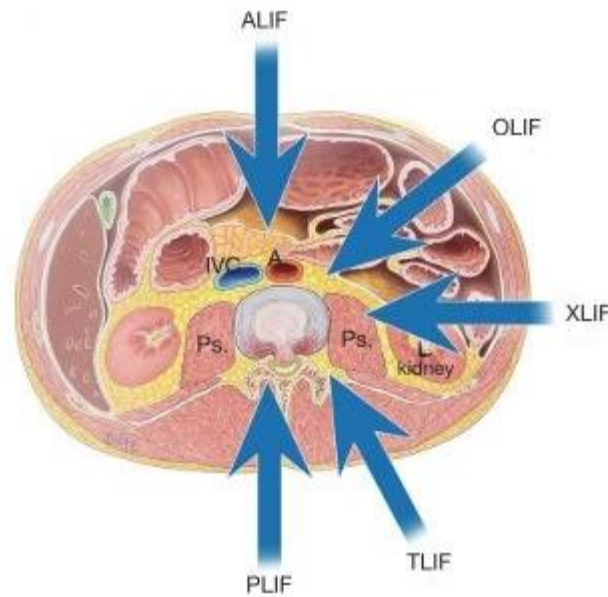


Figure 2.5 Different approaches to interbody fusion for five different procedures. The arrows indicate the path to access the disc space. Adapted from [17].

When the IVD needs to be replaced, a cage is inserted in its place. The device must have certain characteristics to assure distraction and enough support of the axial load. It also grants segmental stability since it causes the ligaments to be under tension. There are two main types of cage design: cylindrical/threaded and box-shaped/rectangular. The first ones are usually inserted as a pair, in the anteroposterior direction. Rectangular cages can be either singular or a pair, and it is possible to introduce bone graft in the interior of the cage or surrounding it [18]. Figure 2.6 shows a representation of a PLIF intervention using two cages and what the disc space looks like when a TLIF cage is inserted and bone graft is applied.

The first cage was created by Bagby to be used in horses. Also known as “Bagby basket”, it was a cylinder of stainless steel that contained autograft and helped fusion. In the 1980s, the device was adapted by Kuslich to be used in humans. It was made of titanium and could be screwed to the endplates [19]. Since then up to this day, different designs have been developed and different materials may be considered. In a FE study of the cervical spine [20], the authors compared the use of a titanium cage with that of a PEEK one. The former, given the increased Young’s Modulus of its material, caused a low relative density in the bone graft when compared with an autograft model or with the PEEK cage. That decrease in density caused by stress shielding may impair fusion.

While fusion excludes the motion that caused pain, stabilizes the segment and permits decompression of the nerve roots [21], the procedure presents some risks, namely accelerated degeneration of the adjacent level, pseudarthrosis and loss of lumbar lordosis when there is an exaggerated distraction [22]. To avoid these effects, there are alternatives to fusion: the disc may be replaced with an artificial one (total disc replacement) or have just its NP replaced. Moreover, semi-rigid or dynamic implants may be used (dynamic stabilization), or the patient can be subjected to Intradiscal Electrothermal Therapy, wherein an electrothermal catheter causes the coagulation of the inflammatory

tissue [14]. However, a review article [21] concluded that there is no certainty that the changes in the adjacent segment are caused by the fact that one of the segments of the spine starts to be rigid and not as a result of the advancement of the degenerative disease.



Figure 2.6 Representation of two possible interbody cages to use in the PLIF (left) and TLIF (right) procedures. Adapted from [23].

Total disc replacement has the advantage of recovering the kinematics of the disc and facet joints. A recent study analyzed the follow-up of 35 patients who underwent this procedure using the Charité III device in the treatment of DDD. The authors found that with this intervention both the Oswestry Disability Index and the Visual Analogue Scale score of the patients improved and the ROM of the adjacent disc decreased. Even though there were no device failures, there were reports of adjacent segment degeneration in one patient and prosthesis subsidence in three. They concluded that, while it may be an alternative to fusion, there was no indication that this approach can protect the contiguous segment in the long term [24]. Figure 2.7 displays the Charité III, used in the study mentioned in this paragraph, and an example of another device: Kineflex.



Figure 2.7 Two examples of devices used in total disc replacement: the Chatité III (left) and the Kineflex (right) [25].

Fusion techniques may be supplemented with posterior fixation. However, it was stated that rigid posterior fixation systems have the disadvantages of resulting in hypermobility of the adjacent segment, thus causing long term degenerative changes and pedicle screw loosening/failure. On the contrary, dynamic fixation systems should reduce the degenerative effects on adjacent segments. Cadaver tests and FE model simulations were performed using rigid or dynamic rods in combination with rigid or dynamic screws (the head comprised a hinged mechanism to allow more flexibility). They concluded that semi-rigid fixation systems convey mobility and thus grant the transmission of load through that segment and the development of a fusion mass. Moreover, the hinged-dynamic screw should permit less stress shielding [26]. Despite this, there have been studies that didn't support the use of Dynesis, a dynamic stabilization system, instead of fusion [27].

## 2.3 Finite Element Models

Tests on cadaveric spines can have limitations such as a limited number of specimens and results influenced by the variability of the spines [26]. Furthermore, in this type of tests, it is only possible to assess the initial stability, which may not be a precise method to predict fusion [18]. On the other hand, computational models are important for the research on spine conditions and diseases [2] as they allow one to easily simulate a variety of loadings and surgical procedures, as well as the effect of different implants.

The first known FE model of the spinal unit, on the left side of Figure 2.8, was made by Belytschko et al. in 1974 [28], who had the goal of studying how the disc reacted under a compressive axial load and how the material properties and variations in geometry influenced its behavior. The model comprised two vertebrae and the IVD, excluding the ALL and PLL. The three components were considered to be symmetric about their respective horizontal center-planes. Cortical and trabecular bone were both modulated as isotropic homogeneous but had different Young's modulus. The NP was represented as incompressible and in a hydrostatic stress state, and the AF fibers were modeled as a single orthotropic material, with Young's modulus changing along the fiber direction. Although simplified, this model allowed the authors to extract the distribution of stress within the IVD, the hydrostatic pressure of the NP and the deformation of the AF and vertebral body.

In 1991, Breau et al. developed a more realistic model from CT scans, including the whole lumbar spine and the S1 vertebra [29]. It included the seven ligaments plus the iliolumbar and the fascia, simulated by uniaxial elements. In Figure 2.8, on the right, two vertebrae and the ligaments joining them are represented. The AF was modeled as a ground substance with collagenous fibers embedded, while the NP was represented as an inviscid fluid. The facet joints were designed as a general moving contact problem.

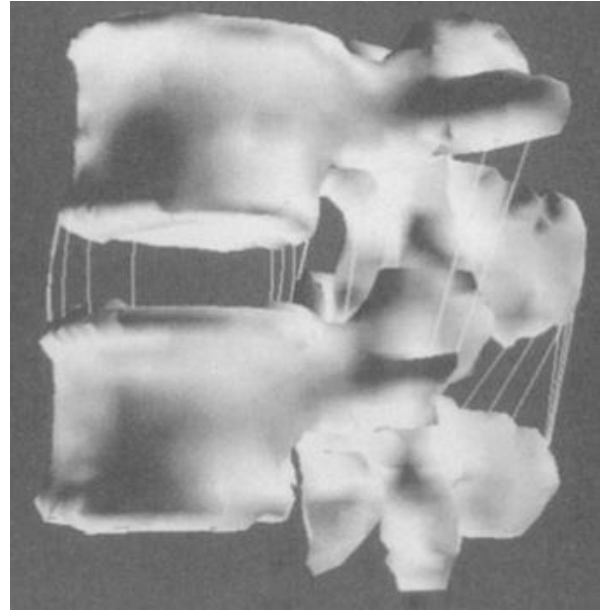
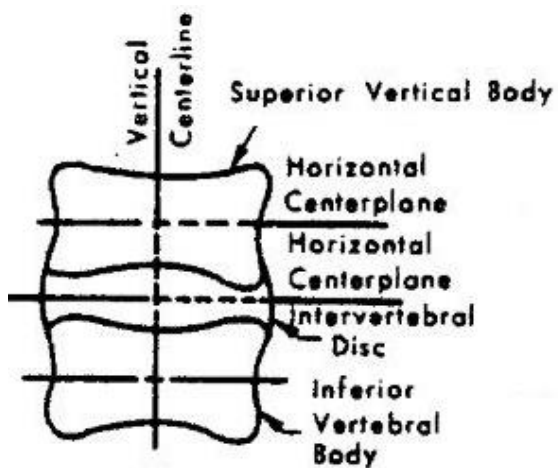


Figure 2.8 Model by Belytschko et al., adapted from [28] (on the left) and one spinal segment, without the IVD, from the Breau et al. model, adapted from [29] (on the right).

Chen et al. built a model of the lumbar spine in 2001, also from CT scan images [7]. It comprised the complete vertebrae, similar to that of Breau et al., and the seven ligaments (ALL, PLL, CL, ISL, SSL, LF and ITL), represented by cable elements, along with the AF fibers. The facet articulations were modeled as 3D contact elements. The complete intact model is depicted in Figure 2.9. ALIF was simulated at different levels and, in some cases, in more than one level. To reproduce the intervention, the IVD of the fusion level was replaced by an interbody bone graft. The model was put under a 10 Nm moment and a 150 N pre-load, firstly to be validated and then to study the ROM and the stress distribution on the adjacent discs.

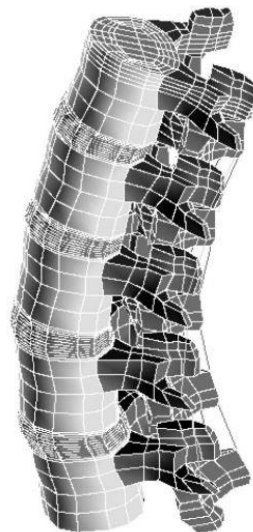


Figure 2.9 Model of the lumbar spine developed by Chen et. al [7].

In 2012, Chen et al. developed an L1-S1 model from CT scans [3]. The lumbar spine was composed of the vertebra, IVD, endplates, and ligaments (ALL, PLL, CL, ISL, LF and ITL) simulated as

tension-only springs. The AF had fibers embedded in its ground substance, and the facet joints were treated as surface-to-surface contact elements, with a friction coefficient of 0.1. In terms of loading, not only did they implement a moment of 10 Nm and a pressure preload of 150 N, but also a compressive force of 400 N to simulate upper-body weight. The muscle forces were considered as well. TLIF was simulated at the L4-L5 level by removing the posterolateral AF, the complete NP, the left facet joint and the LF, modifying the model to mimic decompression and then implementing the cages. The authors considered two cage types, as seen in Figure 2.10: a moon-shaped cage, either placed in the middle or anteriorly, and a diagonal cage. Regarding additional posterior fixation, the models could then be supplemented with bilateral or unilateral pedicle screw fixation. The model with the diagonal cage could also be assisted by a translaminar facet screw or not. The screw-bone interfaces were designed as a full constraint, while the cage-vertebra interface was considered to be a surface-to-surface contact, with a friction coefficient of 0.8. The authors found that unilateral fixation led to a bigger ROM, AF stress at the surgical level and screw-stress. They concluded that, when performing a TLIF procedure with the diagonal cage, unilateral fixation should be supplemented with the facet screw.

In a 2016 study, Ellingson et al. [30] created an L3-sacrum model from CT scans. The AF had seven lamellae, with two layers of fibers oriented at  $\pm 30^\circ$  relative to the horizontal plane. The AF was modeled as neo-Hookean and the NP as linear elastic. The facet joints were simulated by a softened contact parameter that adapted the transmission of force between a pair of nodes exponentially, depending on an initial gap of 0.1 mm. The seven main ligaments were included, and moments of 7 Nm were applied, without an axial preload. To investigate the role of degeneration, they created models with altered material properties for the AF matrix and the NP. A worse degeneration case was found to cause a ROM decrease in all movements. Additionally, they tested what would happen when the spine underwent sequential failure and discovered that progressive failure of the ligaments led to an increase in the ROM.

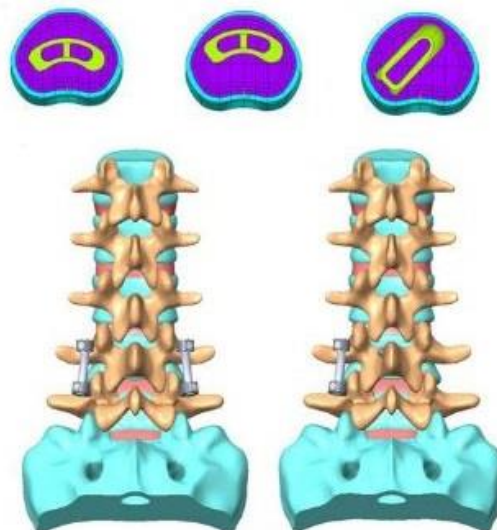


Figure 2.10 On the top, from left to right: moon-shaped cage placed in the middle, moon-shaped cage placed anteriorly and left diagonal cage. On the bottom, the instrumented model with bilateral posterior fixation (left) and unilateral posterior fixation (right). Adapted from [3].

In 2019, Lu et al. built an L3-L5 model, comprising NP's modeled as linearly elastic fluids, AF's represented by a ground substance with layers of inclined fibers with varying strength, and the seven ligaments. They then simulated different interventions at the L4-L5 level. In posterolumbar fusion, the disc was preserved. In the case of TLIF, the left facet joint, the CL, LF, part of the lamina and of the AF and the whole NP were removed, whereas in OLIF and XLIF only the NP and the lateral regions of the AF disappeared. For all of them, bilateral pedicle screws were added, and the interfaces of the instrumentation were modeled as a *Tie* constraint, while the cage-endplate interaction was simulated with a friction coefficient of 0.2. It was concluded that the lumbar interbody fusion techniques permitted greater stability, having shown smaller ROM and stress peaks on the posterior instrumentation than posterolateral fusion. The different cages implemented can be seen in Figure 2.11. TLIF with a banana-shaped cage, placed more anteriorly than the straight one, led to smaller stress peaks in the endplate and trabecular bone. Lastly, the bigger cages used in OLIF and XLIF proved to be better in preventing subsidence and preserving the IVD height [16].

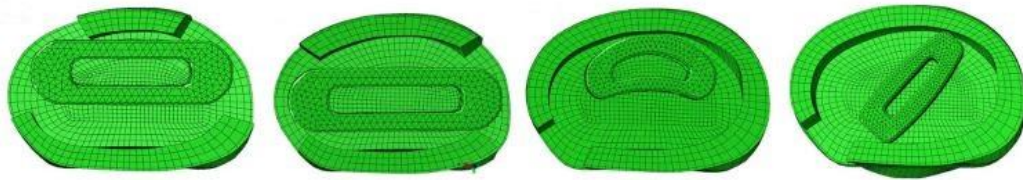


Figure 2.11 Cage positions in the different procedures simulated. From left to right: OLIF, XLIF, TLIF with a banana-shaped cage and TLIF with a straight cage. Adapted from [16].

# Chapter 3

## Methodology

This chapter describes the making of the model, both in terms of its design and implementation, along with the explanation of the most relevant decisions. It also describes the construction of the devices, the instrumented models, and the degenerated models.

### 3.1 Intact model

The model of the complete lumbar vertebra in Figure 3.1 was built by adding the posterior elements to the vertebral body created in past work [8] using Solidworks<sup>®</sup> (Dassault Systèmes SolidWorks Corp., USA). Section images of a vertebra constructed using a CT scan [31] were used to guarantee the new elements were proportional to the vertebral body.

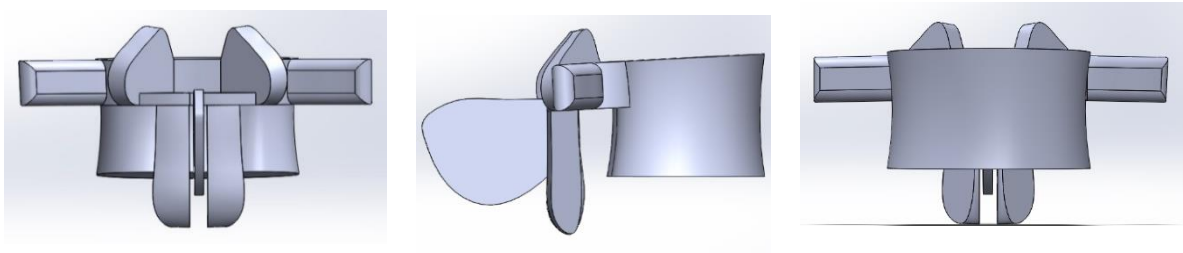


Figure 3.1 Posterior (left), lateral (middle) and anterior (right) view of the model of one lumbar vertebra in Solidworks<sup>®</sup>. The vertebral body was created in [8] and the posterior elements were added in the present work.

After the model of the vertebra was completed, an assembly was created with two identical vertebrae forming an angle of 7 degrees, as done in [8]. The distance between the inferior surface of the upper vertebra and the superior surface of the lower one was made to be such that the average of the anterior and posterior IVD heights was around 10 mm. The IVD was then created by making a *loft* between the two mentioned surfaces and then designing the NP. The same procedure was followed

after adding a third vertebra to the assembly, thus creating the IVD between L4 and L5 and completing the model of the lumbar spine from L3 to L5. As a simplification, the cartilaginous endplates were not distinguished from the bone, as in [7]. The various lengths of the model and IVD areas can be seen in Table 3.1.

Table 3.1 Dimensions of the model.

Vertebral Body	Lateral diameter (mm)	45.0
	Sagittal diameter (mm)	32.5
	Anterior height (mm)	27.5
	Posterior height (mm)	26.0
Intervertebral Disc	Anterior height (mm)	12.6
	Posterior height (mm)	8.5
	Total cross-sectional area (mm <sup>2</sup> )	1268.0
	NP's cross-sectional area (mm <sup>2</sup> )	442.7
Transverse process	Length (mm)	19.4
	Height (mm)	10.0
	Width (mm)	4.9
	Distance peak of one to the peak of the other (mm)	77.4
Spinous process	Sagittal length (mm)	34.0
	Height (mm)	23.5
	Width (mm)	2.0
Superior articular process	Distance from the foramen to the posterior end (mm)	15.5
	Height (mm)	17.2
	Width (mm)	4.3
Inferior articular process	Sagittal length (mm)	8.9
	Height (mm)	26.9
	Width (mm)	7.7
Pedicle	Height (mm)	10.0
Lamina	Height (mm)	2.7
Foramen	Sagittal length (mm)	9.0
	Coronal length (mm)	17.4

The finished model, as seen in Figure 3.2, was saved as .sat and imported to Abaqus<sup>®</sup> (Dassault Systèmes Simulia Corp., USA) as individual parts. Four properties were created (trabecular bone, cortical bone, AF and NP), using the coefficients displayed in Table 3.2, as in [8]. A section was created for each of the properties so they could be attributed to each part.

The AF was defined as a hyperelastic anisotropic material following the Holzapfel formulation [32] as per equation (1), where  $U$  is the strain energy per unit of reference volume;  $C_{10}$ ,  $D$ ,  $k_1$  and  $k_2$

are material parameters that depend on temperature;  $\bar{I}_1$  is the first deviatoric strain invariant;  $J^{el}$  is the elastic volume ratio; N is the number of fibers; and  $\bar{E}_\alpha$  is defined by equation (2), with  $\overline{I_{4(\alpha\alpha)}}$  as a pseudo-invariant.

Considering the parameters used in Abaqus<sup>®</sup> to define de AF,  $C_{10}$  gives the matrix stiffness and D the matrix incompressibility.  $k_1$  and  $k_2$  are related to the fibers, the first with its stiffness and the second with its non-linear behavior. Finally, kappa defines the dispersion of the fibers. It varies between zero (if perfectly aligned) and 1/3 (if randomly distributed).

$$U = C_{10}(\bar{I}_1 - 3) + \frac{1}{D} \left( \frac{(J^{el})^2 - 1}{2} - \ln(J^{el}) \right) + \frac{k_1}{2 \times k_2} \sum_{\alpha=1}^N \{ \exp [k_2 \langle \bar{E}_\alpha \rangle^2] - 1 \} \quad (1)$$

$$\bar{E}_\alpha = \text{kappa} (\bar{I}_1 - 3) + (1 - 3 \text{kappa}) (\overline{I_{4(\alpha\alpha)}} - 1) \quad (2)$$

The behavior of the NP was represented with a hyperelastic isotropic formulation, following the Mooney-Rivlin model [33] in equation (3), where  $C_{10}$ ,  $C_{01}$  and  $D_1$  depend on the temperature; and  $\bar{I}_2$  is the second deviatoric strain invariant. Regarding the parameters in the Abaqus<sup>®</sup> formulation,  $C_{10}$  and  $C_{01}$  account for the shear behavior and  $D_1$  for the compressibility of the material.

$$U = C_{10}(\bar{I}_1 - 3) + C_{01}(\bar{I}_2 - 3) + \frac{1}{D_1} (J^{el} - 1)^2 \quad (3)$$

Afterward, an assembly was formed, and the geometry was merged, retaining the intersecting boundaries. The fibers of the AF were set to make an angle of 35° or 145° with the normal in consecutive layers, as seen in [34]. This was done by assigning an orientation to each AF, of type *discrete*, with y-axis perpendicular to the upper surface and pointing upwards, and x-axis tangent to the outer edge at each point and pointing to the right side of the body.

The ligaments were then added to the model. The choice of the attachment points and the number of ligaments of each type was done based on [34] and [35] (in the case of the ITL, as they were not included in the first one) and is shown in Table 3.3. Between two such points, an axis was created, thus giving the ligament orientation. New parts of the type *wire* were created with the same length as the distance between the two points. When added to the assembly, the ligament was constrained to be parallel to the axis and translated to fit in the correct position. The ligaments were given properties as explained in the next chapter and assigned a section of the type *truss*. They were then meshed as linear trusses, with an element size that produced only one element per ligament. Couplings of the type *continuum distributing* were created at every ligament insertion point, so that it was attached to the surface of the vertebrae model, considering an influence radius of 2.

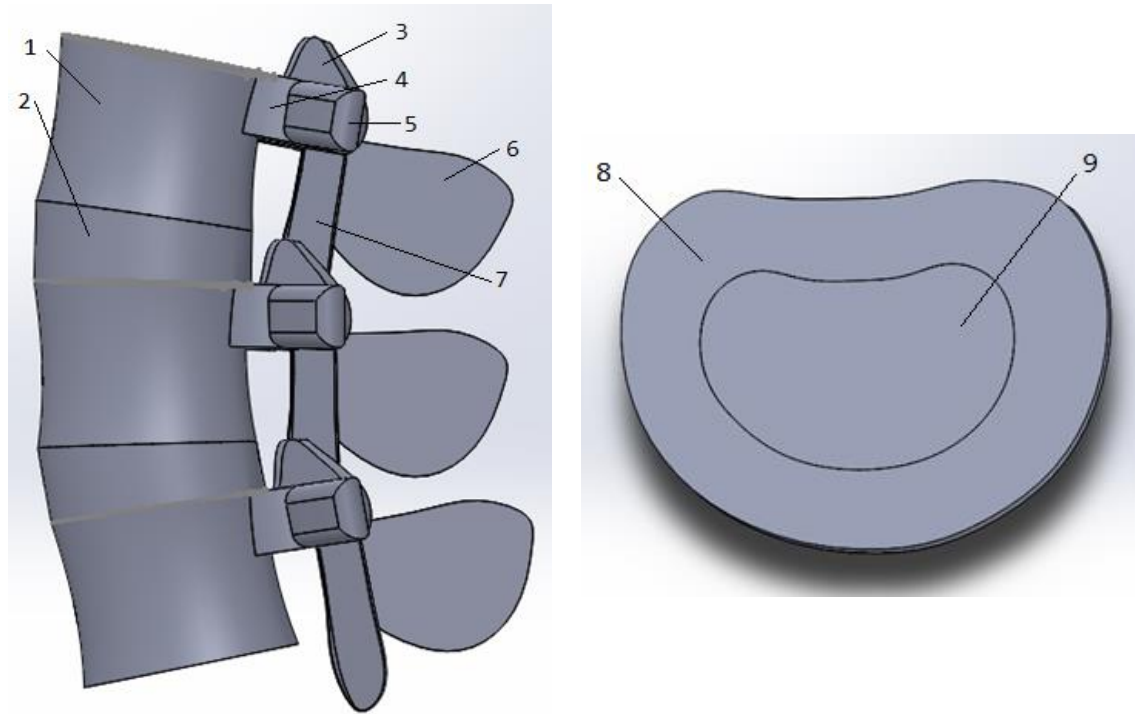


Figure 3.2 Lateral view of the complete model L3 to L5 (left) and superior view of one IVD (right), both created in Solidworks<sup>®</sup>. 1 – vertebral body; 2 – IVD; 3 – superior articular process; 4 – pedicle; 5 – transverse process; 6 – spinous process; 7 – inferior articular process; 8 – AF; 9 – NP.

Table 3.2 Constitutive models and parameters used in Abaqus<sup>®</sup>. All values were taken from [8].

Material	Formulation	Parameters	
Cortical Bone	Linear Elastic	E (MPa)	12000
		$\nu$	0.3
Trabecular Bone	Linear Elastic	E (MPa)	200
		$\nu$	0.315
Annulus Fibrosus	Hyperelastic Anisotropic (Holzapfel)	$C_{10}$	0.315
		$D_1$	0.254
		$k_1$ (MPa)	12
		$K_2$	300
		$\kappa$	0.1
Nucleus Pulposus	Hyperelastic Isotropic (Mooney-Rivlin)	$C_{10}$	0.12
		$C_{01}$	0.03
		$D_1$	0.6667

Table 3.3 Number of ligaments of each type and description of structures they connected in the model.

Ligament	Quantity	Description
ALL	5	Each one is composed of 7 ligaments in a series, with attachment points on the anterior part of the vertebral bodies and IVD.
PLL	3	Each one is composed of 7 ligaments in a series, with attachment points on the posterior part of the vertebral bodies and IVD.
JC	8 on each side	They form a circle, uniting each pair of articular processes.
LF	3	They join the laminae of consecutive vertebrae.
ISL	4	They obliquely connect the spinous processes of consecutive vertebrae.
SSL	3	They associate the posterior part of the spinous processes of consecutive vertebrae.
ITL	2 on each side	They join the transverse processes of consecutive vertebrae.

Two steps were generated with minimum increment and increment size of 0.01 and a maximum increment of 0.1. A referential was created on the upper surface of L3, with origin at its center, x-axis pointing to the right side of the body, y-axis pointing forward and z-axis pointing upward, as seen in Figure 3.3. The loads were applied relative to that referential and a *coupling* was created between the origin and the surface so that they could be distributed equally by all the nodes. In the first step, an FL of 100 N was created. It caused compression and was made to *follow nodal rotation* so that it remained perpendicular to the top surface of L3. The second step contained the propagated FL and a moment of 7.5 Nm to simulate E (positive moment around the x-axis), Flex (negative moment around the x-axis), right/left LB (positive/negative moment around the y-axis) or right/left AR (negative/positive moment around the z-axis).

To restrain the movement of the model, the bottom surface (the base of the L5 vertebral body) was fixed with an *Encastre* boundary condition. To prevent each pair of articular processes from intersecting, in each one of the four cases, a *surface to surface contact* constraint with exponential pressure overclosure was created, as seen in [2]. The parameters were changed until they completely prevented intersection and finally were set to a pressure of 50 N/mm<sup>2</sup> and a clearance of 1 mm. This means that when the distance between the two surfaces is smaller than 1 mm, they start to transmit contact pressure, which increases exponentially as the distance decreases, and reaches 50 N/mm<sup>2</sup> when the distance is zero. Additionally, to prevent each one of the inferior articular processes from intersecting the laminae below, a *surface to surface contact* constraint for tangential behavior was created. Different penalty values were tested until 0.5 completely avoided intersection.

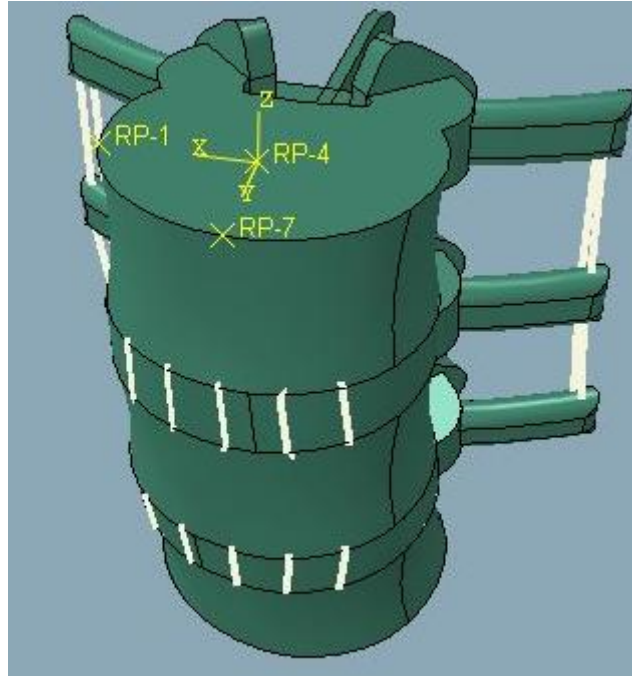


Figure 3.3 Abaqus<sup>®</sup> model of the vertebrae L3 to L5, showing the referential in reference to which the different loads were applied.

### 3.2 Instrumented model

The cage for the OLIF procedure, the screws and the bars that connect the latter were designed in Solidworks<sup>®</sup> following the guidelines of the Medtronic guide [9] and can be seen in Figure 3.4, while their dimensions are presented in Table 3.4.

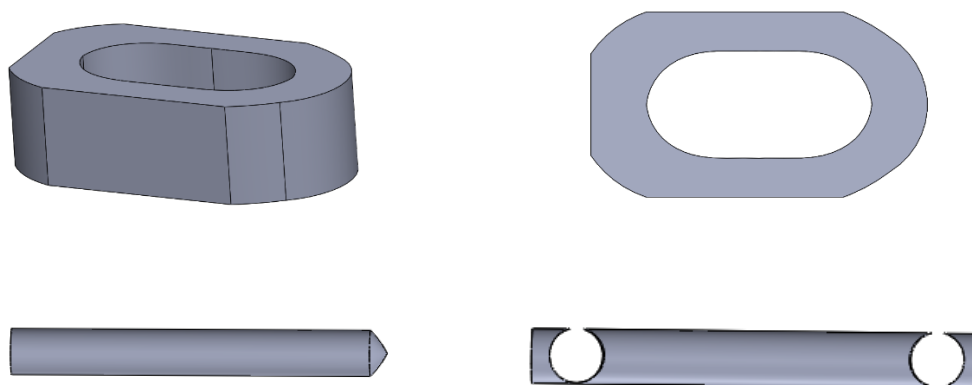


Figure 3.4 Superior-lateral (upper left) and superior (upper right) views of the cage. Model of the screw (bottom left) and bar (bottom right) used in the posterior fixation.

Table 3.4 Dimensions of the cage and posterior fixation devices and material properties given to the FE model.

	Dimensions (mm) [15]		Material
Cage	Length	40	PEEK [36] $E = 3600 \text{ MPa}$ $\nu = 0.38$
	Width	22	
	Height	12	
Screw	Diameter	5.5	Titanium [37] $E = 105000 \text{ MPa}$ $\nu = 0.34$
	Length	45	
Bar	Diameter	5.5	
	Length	45	

The IVD between L4 and L5 was removed and replaced with the cage, thus forming the instrumented model without posterior fixation (cage only), as depicted in Figure 3.5.

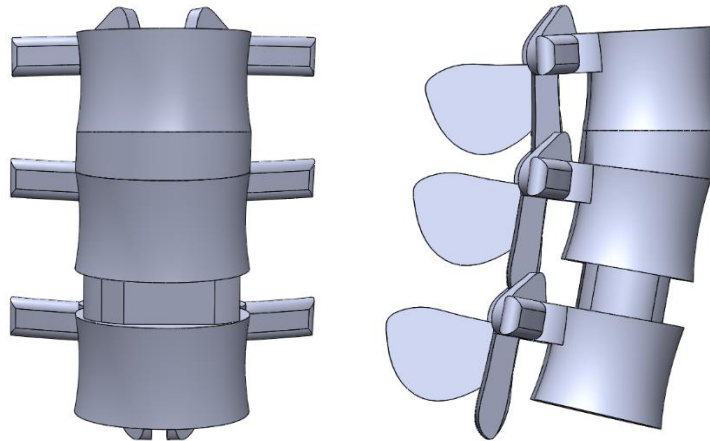


Figure 3.5 Anterior (left) and lateral right (right) view of the L3 to L5 model without posterior fixation and with the cage inserted at the L4-L5 level.

From that one, three other models were created: one with screws inserted through the left pedicles of L4 and L5 and a bar connecting them (unilateral left), one with the screws inserted through the right pedicles (unilateral right) and one with fixation on both sides (bilateral), as portrayed in Figure 3.6.

Each of the four instrumented models was imported to Abaqus<sup>®</sup> and a similar procedure as described in the previous section was performed. All the constitutive parts, with the exception of the cage, were merged to simulate complete osteointegration of the screws and to prevent movement of the screws relative to the bar. The upper and bottom surfaces of the cage were connected to the lower surface of L4 and the upper surface of L5, respectively, with a *Tie* constraint to simulate the long-term integration situation. In the case of the instrumented models, the only constraints implemented to prevent intersection were the ones with exponential behavior between the inferior articular processes of L3 and the superior articular processes of L4.

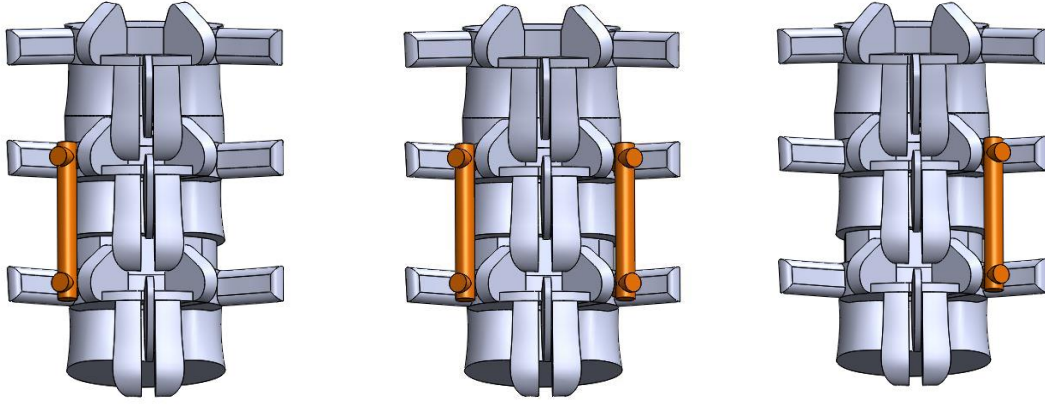


Figure 3.6 Posterior view of the unilateral left (left), bilateral (middle) and unilateral right (right) models.

The models developed are not completely symmetric. Furthermore, the cage was placed medially when considering the anterior-posterior direction but is slightly more shifted to the left. These differences were thought not to influence the angular motion of the spine, as can be seen in the first section of Chapter 5.

### 3.3 Simulation of degeneration

Ruberté et al. [38] simulated two stages of degeneration of the IVD of the L4-L5 level by reducing the disc height and the area of the NP and increasing the laxity of the ALL, PLL and the fibers of the AF. The parameters used to define the degenerated NP and AF can be seen in Table 3.5. In the present study, degeneration was simulated only by changing the properties of the AF and NP in the formulation of the materials, whereas there were no changes in the geometry or properties of the remaining components.

The properties given in Table 3.5 had to be converted to the parameters of the Mooney-Rivlin formulation used in the model, which was achieved using equations (4) to (7), where  $E$  is the Young's Modulus,  $k$  is the bulk modulus and  $\nu$  is the Poisson's ration.

$$E = 6 \times (C_{10} + C_{01}) \quad (4)$$

$$C_{01} = \frac{C_{10}}{4} \quad (5)$$

$$k = \frac{E}{3 \times (1 - 2\nu)} \quad (6)$$

$$D_1 = \frac{2}{k} \quad (7)$$

Table 3.5 Values found in [38] for the mildly and moderately degenerated NP (Young's Modulus and Poisson's ratio) and AF ( $C_{10}$  parameter and Poisson's ratio).

Degree of Degeneration	Nucleus Pulposus		Annulus Fibrosus	
	Young's Modulus (MPa)	Poisson's Ratio	$C_{10}$	Poisson's Ratio
Mild	1.26	0.45	0.5	0.4
Moderate	1.66	0.4	1.13	0.4

Cavalcanti et al. [39] developed a model of the AF, wherein they distinguished four different regions, considering the fiber orientation inside the lamellae varies from ventral to dorsal zones. Their results were then implemented in a complete model of the disc [33].

Since the AF fibers lose part of their ability to withstand pressure, they were modeled in the present work as being laxer in the mildly degenerated case than in the healthy, and further still in the moderately degenerated. Hence the fibers in mild degeneration had the same parameters as the ventral internal region in [39] and in moderate degeneration they had the same values as the dorsal internal.

The final parameters used to simulate degeneration can be seen in Table 3.6.

Table 3.6 Coefficients used in the present work's material formulations of the AF and NP for the healthy, mildly degenerated and moderately degenerated cases.

Degree of degeneration	Annulus Fibrosus				Nucleus Pulposus		
	$C_{10}$	$D_1$	$k_1$ (Mpa)	$k_2$	$C_{10}$	$C_{01}$	$D_1$
Healthy	0.315	0.254	12	300	0.12	0.03	0.667
Mild	0.5	0.32	1.74	43.5	0.168	0.042	0.476
Moderate	1.13	0.14	0.435	8.7	0.221	0.055	0.723

### 3.4 Results Presentation

This work contains the analysis of the ROM, stress and pressure on the disc adjacent to the fused level and stress on the instrumentation, as described in Chapter 5.

The total ROM was obtained by considering a vector uniting two points of the upper L3 vertebra (on the anterior and posterior extremes for E, Flex and AR, and on the lateral extremes for LB) and calculating the angle the vector before motion made with the vector after motion. In the case of the segmental ROM, the one for the L4-L5 level was obtained by measuring the angular motion of the L4 vertebra relative to the constricted L5 one, as described above for the whole model. Then, the L3-L4 segmental ROM was calculated by subtracting the L4-L5 angle from the total ROM, thus achieving the angular motion of the L3 vertebra relative to the one below.

For the adjacent disc, the maximum principal stress was evaluated, allowing a comparison between the non-instrumented model and the instrumented one with adjacent disc healthy or mildly

degenerated. Since the osmotic potential of the NP was not taken into consideration, it was not possible to obtain the intradiscal pressure. However, to specifically analyze the behavior of the NP, the equivalent pressure stress on that component was evaluated to assess how it changed upon the intervention. As for the cage and posterior instrumentation, the parameter chosen was the Von Mises stress since the aim was to check whether they were under risk of failure, and a distinction between tensile and compressive stress was not needed.

# **Chapter 4**

## **Validation**

Before the simulations could be performed, it was necessary to decide the appropriate element size for the mesh of the intact model described in the previous chapter. That choice was done based on the convergence study presented ahead. Furthermore, there is no consensus in the literature about some properties, namely the Young's modulus and cross-sectional area of the ligaments, and the FL, with different papers providing a wide range of values. In order to select them, some tests were made as described ahead.

### **4.1 Convergence study for the mesh**

To decide the appropriate size of the mesh, it was necessary to perform a convergence analysis, to find out for which number of elements the stress value does not depend on the quantity of elements anymore. A vertical downward displacement of 1 mm, around 10% of the average of the IVD heights, was applied on the reference point coupled to the superior surface and meshes of different sizes were generated.

For each mesh, the Von Mises stress was evaluated on a node on the interface between L3 and the upper disc. The fact that the same node was used in all measurements, ensured consistency in the assessment. It was then possible to plot the stress as a function of the number of elements. From the graph in Figure 4.1, it is possible to see that the stress plateaus around a mesh element size of 2 mm. That was the chosen value for all the models used in this work. In the case of the intact model, it led to a total of 158675 linear tetrahedral elements (C3D4).

Partitions were created on some surfaces to choose the ligament attachment points more easily. Additionally, to reduce the number of elements and, as a consequence, the simulation time, the mesh was redone with an increased element growth rate, which allows the elements to be bigger as one moves from the surface inwards. With these two modifications, the number of elements changed to 131760. After adding the ligaments, the final mesh was composed of 131760 elements of type C3D4 and 172 elements of type T3D2, with a total of 27246 nodes.

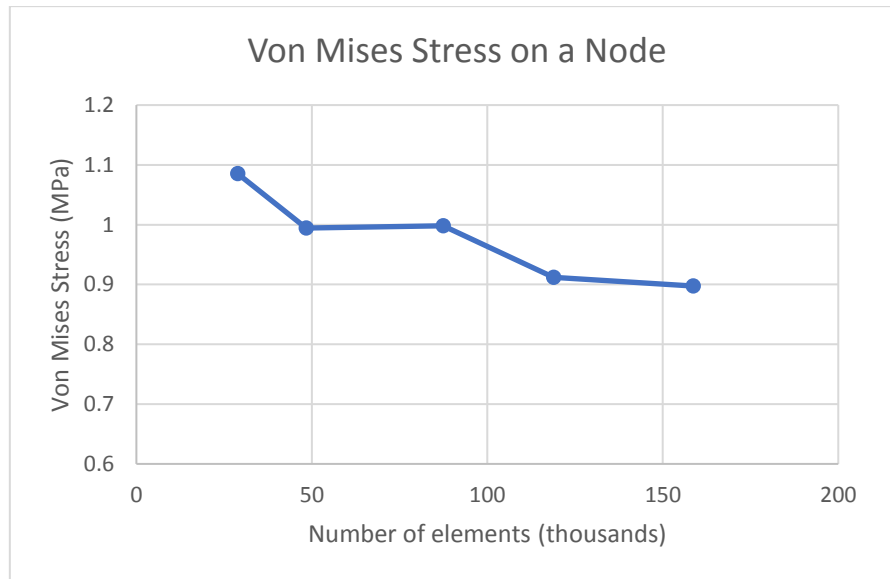


Figure 4.1 Von Mises stress on a node on the interface between the L3 vertebra and the upper IVD, as a function of the number of elements.

## 4.2 Selection of the ligament properties

Given the range of values found in the literature for the Young's modulus and the cross-sectional area of the ligaments, it was necessary to compare the results of the simulations with experimental results, so the best set of properties could be chosen. Heuer et al [40] performed measurements of the ROM in eight cadaver L4-L5 segments with low disc degeneration. In this study, moments of 10, 7.5, 5, 2.5 and 1 Nm were applied to the intact specimens and then each type of ligament was removed sequentially. The ITL were not contemplated since in many of the specimens they were absent after tissue preparation. Even though the model in the present work comprised two spinal units, the total ROM obtained was compared to the results in [40].

Table 4.1 contains the maximum and minimum values of the Young's modulus and cross-sectional area for each ligament. The "divided" values are the cross-sectional areas found in the literature divided by the number of that type of ligament used in the present work.

At first, the parameters chosen were the maximum values in Table 4.1 for all, except the ALL, for which the minimum values were used. In E, the ROM results obtained with these parameters were above the maximum in the literature and so the properties of the ALL had to be increased so that the movement would be restricted. The chosen values were 17 MPa for the Young's Modulus and 14 mm<sup>2</sup> for the cross-sectional area. Flex was then tested and, since some of the ROM were below the literature range, the Young's modulus and areas of the ISL and SSL were decreased, to increase the motion. The ROM calculated for each movement and moment are presented in Table 4.2, as well as the minimum, median and maximum values in [40].

Table 4.1 Range of Young's modulus [30] and cross-sectional areas [41] found in the literature. The values obtained dividing the cross-sectional areas by the number of each type of ligaments in the model of the present study are also presented.

Ligament	Minimum Young's Modulus (Mpa)	Maximum Young's Modulus (Mpa)	Minimum Cross-sectional Area (mm <sup>2</sup> )	Divided Minimum Cross-sectional Area[41][41] (mm <sup>2</sup> )	Maximum Cross-sectional Area (mm <sup>2</sup> )	Divided Maximum Cross-sectional Area (mm <sup>2</sup> )
ALL	15.6	20.0	10.6	2.1	70.0	14.0
PLL	10.0	20.0	1.6	0.5	20.0	6.7
JC	7.5	33.0	19.0	2.4	93.6	11.7
LF	13.0	19.5	40.0	13.3	114.0	38.0
ISL	9.8	12.0	12.0	3.0	60.0	15.0
SSL	8.8	15.0	6.0	2.0	59.8	19.9
ITL	12.0	58.7	1.8	0.9	10.0	5.0

Table 4.2 Values of the ROM in degrees: minimum, median and maximum found in the literature [11]. In blue, the values obtained in the simulation.

Movement	Moment (Nm)	Minimum ROM in the Literature (deg)	Median ROM in the Literature (deg)	Maximum ROM in the Literature (deg)	ROM of the model (deg)
E	10	3.83	4.92	5.75	5.92
	7.5	3.17	4.1	4.92	4.75
	5	2.50	3.14	4.08	3.45
	2.5	1.08	1.89	2.83	1.92
	1	0.33	0.66	1.67	0.79
Flex	10	4.90	7.14	9.46	6.16
	7.5	4.15	6.19	8.13	4.81
	5	3.32	5.02	6.80	3.33
	2.5	1.66	3.13	4.48	1.71
	1	0.42	0.75	1.49	0.69
Left AR	10	1.54	3.45	4.32	5.00
	7.5	1.17	2.7	3.70	4.06
	5	0.74	1.88	2.84	2.95
	2.5	0.31	0.98	1.79	1.61
	1	0.12	0.36	0.74	0.68
Right LB	10	4.52	6.12	7.13	8.58
	7.5	3.97	5.15	6.51	6.81
	5	3.29	4.19	5.52	4.81
	2.5	2.05	2.81	3.78	2.51
	1	0.74	1.28	1.74	0.99

As shown in Table 4.2, the ROM obtained was within the literature range for all the moments in Flex and all of them, except for 10 Nm, in E. When simulating LB, valid ROM were obtained for the three lowest moments, whereas in AR only the two lowest ones were within range. The highest difference to the maximum value of the range was found for an LB of 10 Nm. The ligament properties used to achieve these results and throughout the rest of the work are summarized in Table 4.3.

Table 4.3 Ligament properties after validation.

Ligament	Young Modulus (MPa)	Cross-sectional Area of each ligament (mm <sup>2</sup> )
ALL	17.0	14.0
PLL	20.0	6.7
CL	33.0	11.7
LF	19.5	38.0
ISL	10.0	10.0
SSL	10.0	14.0
ITL	58.7	5.0

### 4.3 Selection of the Follower Load

The implementation of the FL in the literature varies, with some authors mentioning only the application of pure moments [42], and others using an FL with values ranging from 100 N [43] to 1000 N [2]. In the case of [44], the loading case actually differed for distinct motions. For the standing, Flex and E cases, a bodyweight of 260 N, applied vertically, was considered at the same time as an FL of 200 N, simulating the action of the muscles; whereas for AR only an FL of 500 N was contemplated.

Table 4.4 shows the ROM obtained for the four movements when the model was under different moment and FL combinations. As shown, the cases of no FL and 100 N FL had the highest number of simulations within the range in the literature. Although in [40] the tests were done with no FL and using only the L4-L5 segment, it was the most similar study to the present work and thus was chosen to validate the selection of the FL.

To choose between the 0N FL and the 100 N FL cases, the distance of the obtained results to the lower or upper limit of the range in the literature (when the value was smaller or bigger than that range, respectively) was compared. The 100 N FL case showed better results in E, Flex and LB and hence was chosen for all the subsequent tests.

Table 4.4 ROM, in degrees, obtained for the model subjected to the moment and FL indicated, in E, Flex, AR and LB.

Extension					
Moment (Nm)	FL 0 N	FL 100 N	FL 200 N	FL 300 N	FL 500 N
1	5.92	5.02	4.11	3.18	0.71
7.5	4.75	3.84	2.91	1.78	0.90
5	3.45	2.52	1.44	0.14	2.59
2.5	1.92	0.87	0.66	2.03	4.07
1	0.79	0.57	1.87	2.99	4.89
Flexion					
Moment (Nm)	FL 0 N	FL 100 N	FL 200 N	FL 300 N	FL 500 N
10	6.16	7.10	7.93	8.67	9.91
7.5	4.81	5.85	6.77	7.58	8.93
5	3.33	4.47	5.49	6.38	7.83
2.5	1.71	2.95	4.04	5.02	6.65
1	0.69	1.97	3.14	4.18	5.93
Axial Rotation					
Moment (Nm)	FL 0 N	FL 100 N	FL 200 N	FL 300 N	FL 500 N
10	5.00	5.24	5.56	5.95	6.82
7.5	4.06	4.36	4.78	5.27	6.34
5	2.95	3.36	3.93	4.58	5.91
2.5	1.61	2.23	3.08	3.95	5.57
1	0.68	1.58	2.65	3.67	5.45
Lateral Bending					
Moment (Nm)	FL 0 N	FL 100 N	FL 200 N	FL 300 N	FL 500 N
10	8.58	8.42	8.20	7.89	7.17
7.5	6.81	6.32	6.54	6.27	5.62
5	4.81	4.81	4.68	4.46	3.91
2.5	2.51	2.61	2.55	2.39	2.01
1	0.99	1.11	1.06	0.99	0.88



# ***Chapter 5***

## **Results and Discussion**

This chapter consists of the results obtained in the various simulations, considering an FL of 100 N, as mentioned in Validation, and a moment of 7.5 Nm, as referred in Methodology. Four groups of models can be recognized: the non-instrumented case, with both discs healthy, the non-instrumented case with varying degrees of degeneration, the different instrumented constructs with adjacent disc healthy and the different instrumented constructs with adjacent disc mildly degenerated. They were analyzed in terms of the ROM and stress and the results were compared with relevant literature.

### **5.1 Range of Motion**

#### **5.1.1 Degenerated models**

To understand the implications of degeneration on the biomechanics of the spine, different combinations of IVD state were considered, as presented in Table 5.1.

Table 5.1 Combinations of IVD states considered in the analysis.

Number	State of the L3-L4 IVD	State of the L4-L5 IVD
(1)	Healthy	Healthy
(2)	Healthy	Mild
(3)	Mild	Mild
(4)	Healthy	Moderate
(5)	Mild	Moderate

If the degeneration increases as one moves from case (1) to case (5), for E, Flex and LB the lumbar spine became less mobile (total ROM decreased) from the healthy case to the most severe case, as demonstrated in Table 5.2. On the contrary, AR increased the ROM for the case where only the lower disc presents mild degeneration and even more when both discs are mildly degenerated. For the cases

with the lower disc moderately degenerated, the ROM decreased when comparing cases (4) and (5) to their equivalents with bottom disc mildly degenerated: cases (2) and (3), respectively.

Considering the case of the two healthy discs as the norm, the highest percentage changes were found for AR (the highest being 56% for case (3), followed by 45% for case (5) ). The percentage change was also considerable for case 5, in Flex (22%) and LB (17%).

Table 5.2 ROM, in degrees, obtained for the four movements for different combinations of degeneration states of the discs. The values in gray are the percentage changes relative to the healthy case, (1).

Movement	Case (1) (deg)	Case (2) (deg)	P.C. (%)	Case (3) (deg)	P.C. (%)	Case (4) (deg)	P.C. (%)	Case (5) (deg)	P.C. (%)
E	3.84	3.82	-0.5	3.79	-1.1	3.58	-6.7	3.56	-7.3
Flex	5.85	5.56	-5.1	5.24	-10.4	4.89	-16.5	4.57	-21.9
Left AR	4.36	5.47	25.4	6.80	56.1	4.97	14.0	6.31	44.8
Right LB	6.72	6.63	-1.3	6.49	-3.4	5.69	-15.3	5.56	-17.3

Table 5.3 and Table 5.4 contain the segmental ROM of the upper and bottom spinal units, respectively. Comparing the models with an upper disc healthy and the three possible states of the bottom disc, the results show that, with degeneration, there was an increase in the L3-L4 ROM in E, Flex and LB, and a decrease for AR. However, the percentage changes when taking the healthy model as the norm were small to the point of being negligible. The ROM of the degenerated L4-L5 segment decreased up to 15%, 35% and 34% in E, Flex, and LB, respectively, as degeneration progressed. For AR, the spinal unit was more mobile when the bottom disc was only mildly degenerated than in the case of moderate degeneration.

Table 5.3 Segmental ROM of the L3-L4 spinal unit, in degrees, obtained for the four movements, with the upper disc healthy and the three possible bottom disc states. The values in gray are the percentage changes relative to the healthy case, (1).

Movement	Case (1) (deg)	Case (2) (deg)	P.C. (%)	Case (4) (deg)	P.C. (%)
E	2.08	2.08	0.1	2.10	0.7
Flex	2.99	3.01	0.7	3.04	1.7
Left AR	2.26	2.23	-1.1	2.19	-3.0
Right LB	3.66	3.67	0.3	3.69	0.8

In the present work, with increased degeneration the spine became less mobile for E, Flex and LB (the ROM of the degenerated models is smaller than that of the healthy model). However, in AR there was an increase in ROM as more severe cases of degeneration were considered.

This trend in AR was also found in [45], a study where the ROM for this motion was measured in cadaver spinal units at different levels (T12-L1 to L4-L5) to establish a relationship between the ROM and the stage of degeneration, as perceived in different classification scales.

Table 5.4 Segmental ROM of the L4-L5 spinal unit, in degrees, obtained for the four movements, with the upper disc healthy and the three possible states of the bottom disc. The values in gray are the percentage changes relative to the healthy case, (1).

Movement	Case (1) (deg)	Case (2) (deg)	P.C. (%)	Case (4) (deg)	P.C. (%)
E	1.75	1.73	-1.2	1.48	-15.4
Flex	2.86	2.55	-11.1	1.85	-35.4
Left AR	2.10	3.24	54.0	2.78	32.2
Right LB	3.06	2.96	-3.3	2.01	-34.4

In [38] it was found that the angular motion increased in the upper adjacent level for all motions, whereas in the present study, ROM decreased for AR and all the percentage changes, comparing the degeneration values to the healthy ones, were rather low. For the degenerated level (L4-L5), [38] found a decrease of the ROM for only AR and LB, while here the ROM increased for AR and decreased for the remaining motions. However, a direct comparison cannot be made since, in the mentioned paper, the model comprises the spine from L1 to S1. That might also explain why there is a change in the total ROM with degeneration in the present study and in [38] the total ROM does not vary, having more adjacent levels to compensate for the changes at the degenerated level.

In [42] an L3-L4 model was created to study the effects of degeneration on a segment. They tested three degrees of degeneration (mild, moderate and severe) with decreasing disc heights and increasing NP compressibility, from healthy to severely degenerated, while the properties of the AF were kept constant. They found that ROM increased in all movements from healthy to mildly degenerated discs. With degeneration further increasing, E, Flex and LB presented a ROM decrease compared with mild, whereas in AR it increased for moderate degeneration. In the present work, the ROM of the degenerated segment decreased for E, Flex and LB. This might be because, in the present work, with increasing degeneration, the ground substance of the AF became more rigid, while in [42] only the NP is taken into account and the length of the AF fibers was changed with the decrease in disc height. Furthermore, the latter implemented changes in the ligament length, adding to the fact that it considered an isolated segment.

### 5.1.2 Instrumented models

Instrumentation produced a reduction of the total ROM compared to the healthy (non-instrumented) model for all motions, as can be seen in Table 5.5. Furthermore, the reduction was

stronger for unilateral fixation compared to cage only, and even more so for bilateral fixation, except for right LB, where the bilateral and unilateral left models produced the same ROM.

Table 5.5 ROM, in degrees, of the healthy model and the four instrumented ones. The values in gray are the percentage changes relative to the healthy case.

Movement	Healthy (deg)	Cage only (deg)	P.C. (%)	Unilat. Left (deg)	P.C. (%)	Unilat. Right (deg)	P.C. (%)	Bilateral (deg)	P.C. (%)
E	3.84	2.56	-33.1	2.37	-38.1	2.40	-37.4	2.31	-39.7
Flex	5.85	3.68	-37.2	3.57	-39.0	3.56	-39.2	3.49	-40.4
Left AR	4.36	2.47	-43.2	2.45	-43.8	2.44	-44.0	2.42	-44.4
Right LB	6.72	3.98	-40.7	3.91	-41.8	3.96	-41.0	3.91	-41.8
Right AR				2.37	-45.6	2.38	-45.4		
Left LB				3.96	-41.1	3.92	-41.6		

For E, the bilateral model caused a ROM percentage change, when comparing to the healthy model, of approximately 40%, while the cage only model originated a reduction of only 33%. The effect of the unilateral model was similar to that of the bilateral one. In the cases of Flex, AR, and LB, the results of all the models were similar.

The right AR and left LB of the unilateral models were compared to left AR and right LB of the healthy one, respectively. There wasn't a significant difference between bending or rotating to the left or to the right for each unilateral construct. The two unilateral models behaved similarly when comparing the cases where both are rotating/bending to the side of the instrumentation or to the opposite side.

For the L3-L4 segment, as can be seen in Table 5.6, in E and Flex, the segmental ROM increased relative to the healthy case for all constructs, but that gain decreased as the instrumentation became more restrictive (from no posterior fixation to bilateral). For left AR, all the constructs had ROM smaller than the healthy, with very small percentage changes. In right LB the ROM was greater than in the healthy case for all constructs, however, the unilateral left model caused the smallest increase, followed by the bilateral one, the unilateral right one and finally the cage only one. The unilateral models showed similar results when bending or rotating to the same side of fixation or to the opposite side.

Table 5.6 ROM of the L3-L4 segment, in degrees, for the healthy and instrumented cases. The values in gray are the percentage changes relative to the healthy case.

Movement	Healthy (deg)	Cage only (deg)	P.C. (%)	Unilat. Left (deg)	P.C. (%)	Unilat. Right (deg)	P.C. (%)	Bilateral (deg)	P.C. (%)
E	2.08	2.21	6.1	2.16	3.5	2.18	4.6	2.15	3.4
Flex	2.99	3.32	11.0	3.31	10.9	3.30	10.5	3.29	10.0
Left AR	2.26	2.24	-0.8	2.23	-1.1	2.23	-1.1	2.23	-1.3
Right LB	3.66	3.82	4.5	3.77	3.1	3.81	4.3	3.79	3.6
Right AR				2.16	-4.1	2.16	-4.1		
Left LB				3.82	4.5	3.79	3.5		

Table 5.7 shows that the instrumentation caused a considerable decrease in the segmental ROM of the L4-L5 spinal unit. For all the motions this restriction of movement was bigger in the unilateral model than in the cage only one, and even greater for the bilateral model. The movement that was more successfully constrained was LB, with a change of approximately 95 % for the cage only and unilateral constructs and 96 % for the bilateral model. The three types of fixation caused similar results in AR and LB, while the result for Flex appeared to depend more on the type of fixation. Extension granted the highest disparity among models, with the cage only case decreasing the ROM in around 80% and the bilateral model managing to reduce it by 91%.

Table 5.7 ROM of the L4-L5 segment, in degrees, for the healthy and instrumented cases. The values in gray are the percentage changes relative to the healthy case.

Movement	Healthy (deg)	Cage only (deg)	P.C. (%)	Unilat. Left (deg)	P.C. (%)	Unilat. Right (deg)	P.C. (%)	Bilateral (deg)	P.C. (%)
E	1.75	0.36	-79.7	0.22	-87.6	0.22	-87.3	0.16	-90.9
Flex	2.86	0.36	-87.5	0.26	-91.1	0.26	-91.0	0.20	-93.0
Left AR	2.10	0.24	-88.7	0.22	-89.7	0.21	-90.1	0.20	-90.7
Right LB	3.06	0.16	-94.7	0.14	-95.4	0.15	-95.2	0.12	-96.1
Right AR				0.21	-90.1	0.22	-89.8		
Left LB				0.14	-95.4	0.14	-95.5		

Chen et al. [7] created an L1-L5 model to understand the changes in the stress on the adjacent disc after ALIF, where this procedure was simulated by replacing the IVD with an interbody graft. This graft had a Young's modulus of 3500 MPa, similar to that of the PEEK cage used in the present study. While the decrease of the total ROM after fusion was similar in E (36% in the literature and 33% in the present work), the first showed smaller decreases for the other motions (26%, 29% and 10% in Flex, AR and LB, respectively, versus 37%, 43% and 41% in this work). This discrepancy may be due to the fact that the overall lumbar ROM is less affected by one-level fusion than a model of only two segments.

In the present study, as expected, the bilateral posterior fixation achieved the highest ROM reduction amongst the three constructs, followed by the unilateral fixation. The movement for which differences in fixation had the strongest impact was E, whereas the other three didn't show a strong disparity among models.

Considering the segmental ROM, instrumentation caused a severe reduction at the fused level, as was predicted since the goal of the procedure is to stabilize the segment as much as possible. Although there were no percentage changes of 100 %, which means the instrumented spinal unit kept some motion for all cases, the percentage changes went from a 79.7 % decrease, for the cage only model in E, to a 96.1 % decrease for the bilateral model in LB.

A study simulating TLIF in a L1-S1 spine [3] found that, at the level of the intervention, the ROM was smaller in the bilateral case (when compared to the values of the unilateral, 15 to 22% in E, 26 to 32% in right AR and 27 to 59% in right LB). In the present study also, bilateral posterior fixation achieved

smaller L4-L5 ROM in all movements, with a similar ROM percentage change in E (27 to 29%, relative to the values of the unilateral fixation). However, it had also a significant decrease in Flex (22%), a non-significant decrease for AR and a less intense reduction for LB (15 to 19%).

In another study [46], the authors created an L3-L5 model to compare bilateral posterior fixation to the unilateral one in TLIF when applying a moment of 10 Nm and no FL. For all movements they found no ROM differences for the adjacent segment compared to the intact model, as happened in the present study (the highest percentage change was 11% for the cage only model in Flex).

Conversely, there was a great reduction of motion at the fusion level in [46]. Moreover, in the literature, the two types of fixation were considered to differ in terms of stability. Flex was associated with a greater ROM decrease than E, but this may be because the crescent-shaped cage was placed more anteriorly. In the present study also, the L4-L5 segment suffered a great reduction in the segmental ROM, bigger for Flex than E. At the same level, the cage only model performed differently from the models with posterior fixation, when comparing the reduction all of them caused relative to the intact case. Although the unilateral and bilateral models presented a similar reduction of the intact ROM, the values of the bilateral case were 27-29% smaller than those of the unilateral fixation (relative to the values of the latter), confirming the instability mentioned in the literature.

On the level of instrumentation, when bending to the side of fixation, [46] reported a less than 50% ROM reduction for the unilateral model, while bilateral fixation reduced the ROM in more than 90%. However, when bending to the opposite side, the ROM reduction of the unilateral model was greater than 75%. In the present study the ROM decrease at fusion level, for bilateral and unilateral fixation was similar, regardless of bending to one side or the other. The ROM obtained for the bilateral model was 17% smaller than that of the cage only model, when compared to the latter.

In AR, the unilateral fixation in [46] managed a ROM reduction over 63%, whereas the decrease for bilateral was more than 90%. In the present study, AR was the movement with the smallest difference from model to model. In addition, similar results were achieved when rotating to the left or to the right.

### **5.1.3 Degenerated instrumented models**

Comparing the degenerated instrumented models with their healthy equivalents, as shown in Table 5.8, there was a decrease of the ROM for E, Flex and LB (less than 1%, around 10%, and approximately 3.5%, respectively). However, when undergoing AR, the ROM of the degenerated model exceeded that of the healthy one by around 57%. There were no significant changes between rotating or bending to the left or right. The two unilateral models had very similar outcomes.

Since the cage can be a replacement for a damaged disc, Table 5.9 shows a comparison between the model with healthy upper disc and bottom disc moderately degenerated and the model with a healthy disc and the cage. Similarly, Table 5.10 presents the comparison in the case of the non-instrumented model having the upper disc mildly degenerated. For Flex, the instrumentation restricted the movement more when the adjacent disc was mildly degenerated. On the contrary, AR was more restrained when the adjacent disc was healthy. In E and LB, instrumentation had very similar effects for both cases.

Table 5.8 ROM, in degrees, of the instrumented models with the L3-L4 mildly degenerated, for all the motions. The values in gray are the percentage changes relative to the instrumented models with healthy upper IVD.

Movement	Cage only (deg)	P.C. (%)	Unilat. Left (deg)	P.C. (%)	Unilat. Right (deg)	P.C. (%)	Bilateral (deg)	P.C. (%)
E	2.55	-0.7	2.35	-0.8	2.38	-0.7	2.30	-0.7
Flex	3.34	-9.2	3.23	-9.6	3.22	-9.5	3.15	-9.7
Left AR	3.87	56.4	3.85	57.0	3.83	57.2	3.81	57.2
Right LB	3.84	-3.6	3.77	-3.4	3.82	-3.6	3.77	-3.5
Right AR			3.76	58.5	3.76	58.2		
Left LB			3.79	-4.4	3.76	-4.2		

Table 5.9 ROM, in degrees, for degeneration case (4) and the cage only model with the adjacent disc healthy, for all motions. The values in gray are the percentage changes relative to degeneration case (4).

Movement	Case (4) (deg)	Cage only (deg)	P.C. (%)
E	3.58	2.56	-28.3
Flex	4.89	3.68	-24.8
Left AR	4.97	2.47	-50.2
Right LB	5.69	3.98	-30.0

Table 5.10 ROM, in degrees, for degeneration case (5) and the cage only model with the adjacent disc mildly degenerated, for all motions. The values in gray are the percentage changes relative to degeneration case (5).

Movement	Case (5) (deg)	Cage only (deg)	P.C. (%)
E	3.56	2.55	-28.5
Flex	4.57	3.34	-27.0
Left AR	6.31	3.87	-38.7
Right LB	5.56	3.84	-30.9

In the L3-L4 segment, as seen in Table 5.11, AR presented a considerable change, with values 62-63% greater in the degenerated case. Flex and LB presented a decreased ROM compared to the healthy instrumented model, though the change was less appreciable than that of AR. Extension increased for the cage only model and decreased for the other three constructs.

The changes in the segmental L4-L5 ROM, as seen in Table 5.12, were not relevant compared to the values obtained for the same instrumentation with the adjacent disc healthy, except for E in the cage only model.

Table 5.11 ROM of the L3-L4 segment, in degrees, of the instrumented models with the adjacent disc mildly degenerated. The values in gray represent the percentage changes relative to the instrumented models with the adjacent disc healthy.

Movement	Cage only (deg)	P.C. (%)	Unilat. Left (deg)	P.C. (%)	Unilat. Right (deg)	P.C. (%)	Bilateral (deg)	P.C. (%)
E	2.43	9.8	2.14	-0.9	2.16	-0.8	2.14	-0.8
Flex	2.97	-10.4	2.97	-10.4	2.96	-10.4	2.95	-10.4
Left AR	3.64	62.5	3.63	62.7	3.63	62.7	3.62	62.4
Right LB	3.68	-3.8	3.64	-3.6	3.67	-3.8	3.65	-3.6
Right AR			3.56	64.3	3.55	64.1		
Left LB			3.65	-4.6	3.62	-4.4		

Table 5.12 ROM of the L4-L5 segment, in degrees, of the instrumented models with the adjacent disc mildly degenerated. The values in gray represent the percentage changes relative to the instrumented models with the adjacent disc healthy.

Movement	Cage only (deg)	P.C. (%)	Unilat. Left (deg)	P.C. (%)	Unilat. Right	P.C. (%)	Bilateral (deg)	P.C. (%)
E	0.12	-66.4	0.22	-0.1	0.22	0.1	0.16	0.0
Flex	0.36	1.5	0.26	1.6	0.26	1.6	0.20	1.7
Left AR	0.23	-1.2	0.22	-0.7	0.21	-1.9	0.19	-1.6
Right LB	0.16	-0.1	0.14	0.2	0.15	0.2	0.12	0.6
Right AR			0.20	-2.0	0.21	-1.1		
Left LB			0.14	0.6	0.14	0.4		

Considering the total ROM, the degenerated models presented values similar to the healthy case in E and LB, a decrease of around 10% in Flex and an increase of approximately 57% in AR. This is in accordance with the comparison between the cage constructs and the non-instrumented models with the bottom disc moderately degenerated. As mentioned above, for Flex the instrumentation restricted the motion more for the mildly degenerated disc, while in AR it was more restricted in the healthy case. However, the differences in the percentage changes on Table 5.9 and Table 5.10 were very small compared to the discrepancy between 10 and 57%.

The percentage changes relative to the instrumented models with healthy adjacent discs showed that, with the exception of E for the cage only model, the state of the upper disc did not affect the ROM at the fusion level. For the L3-L4 segment, the case of the mildly degenerated disc presented a smaller ROM in LB and Flex, but a considerable increase in ROM for AR. This means that the spine only became less stable in the presence of an adjacent mildly degenerated disc in AR.

A recent study investigated the alterations at the proximal adjacent segment after a PLIF procedure, for different stages of degeneration of the adjacent disc [47]. The PLIF procedure was simulated on an L3-L5 model: the L4-5 disc was replaced by a cage supplemented with bilateral

posterior fixation. The NP formulation was the same as in the present work and the AF was modeled with a Mooney-Rivlin formulation, with embedded fibers. The most severe case of degeneration in [47] had an NP formulation similar to the mild degeneration case in the present work, and thus the two can be compared. In the literature, there was a ROM decrease for all motions (54% in E/Flex, 38% in LB and 17% in AR). The present work showed very different results: the ROM in E had a variation of less than 1%, in Flex and LB it decreased by 10% and 4%, respectively, and in AR it increased 62%. AR followed the same trend as in [45], as mentioned in the discussion of the degeneration of the non-instrumented models. The relevant decrease of the ROM for all motions in [47] may have been caused by the fact that the IVD height was reduced by 33%, while on the present work it was kept the same as in the healthy model. In fact, in a study with the aim of discovering the impact of disc height in the mechanical behavior of the lumbar spine [48], a simplified L2-L3 model with no posterior elements or ligaments was built. They observed that, for a 50% increase of the disc height, when applying the same axial compressive force, the posterolateral disc bulge increased 42%. This means that the disc height plays a role in the biomechanics of the segments.

## 5.2 Stress

### 5.2.1 Adjacent disc

For E, there were no noticeable changes in the stress profile for the different types of instrumentation used. As the spine bent backwards (around the x axis), a zone of high compression formed in the posterior AF and a zone of high tension appeared in its anterior part. Most of the NP was under tension. The bilateral model was the only one that produced a noticeable change of the tensile maximum principal stress, having had an increase of 50% compared to the non-instrumented healthy model. All the instrumented models increased the compressive stress on the adjacent disc, from an increase of 20% by the unilateral left to increases of 33-36% by the other three.

When considering the degenerated instrumented models, for all the types of instrumentation, the degenerated disc was subjected to lower tensile stress than the healthy one, which can be seen in Figure 5.1 since the zone of highest tensile stress in the anterior AF almost disappeared in the degenerated disc. Compared to the values obtained for the instrumented constructs with the adjacent disc healthy, the maximum tensile stress decreased close to 20% for the cage only and unilateral models and 37% for the bilateral one. The maximum compressive stress decreased around 4% for all, except the unilateral left, for which it increased 12%.

S, Max. Principal  
(Avg: 75%)

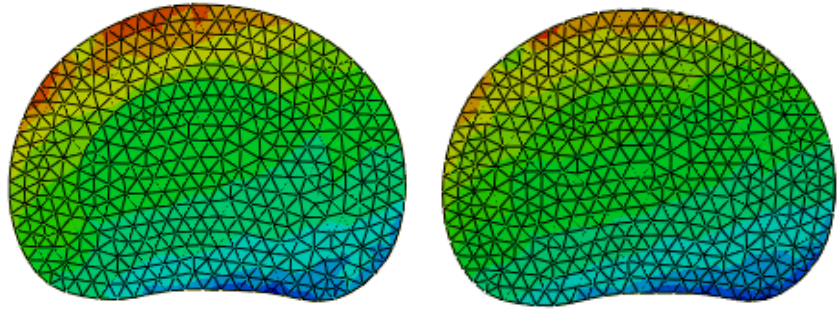
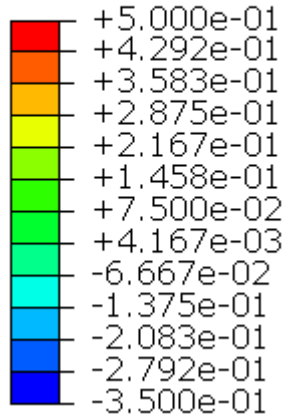


Figure 5.1 Maximum principal stress in the L3-L4 healthy (left) and mildly degenerated (right) disc when the bilateral model is subjected to E.

In the case of Flex, the high compression zone was localized in the anterior part of the AF, close to the NP. All the instrumented models behaved similarly, with an increase of the tensile stress in the posterior part of the AF, particularly on the right side, when compared to the non-instrumented healthy model, as per Figure 5.2. The unilateral right model had the smallest increase in maximum tensile stress (56%), followed by the cage only, the unilateral left and finally the bilateral one, which almost doubled the maximum of the healthy model. As for the compressive stress, the unilateral right and cage only models caused an increase of 13-15%, while the unilateral left made no substantial change and the bilateral one caused a reduction of the maximum.

S, Max. Principal  
(Avg: 75%)

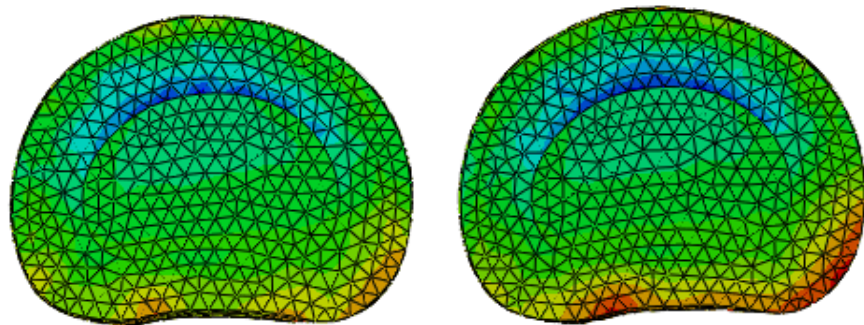
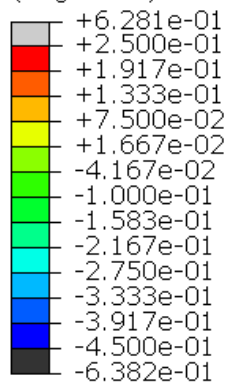


Figure 5.2 Maximum principal stress on the L3-L4 disc of the non-instrumented healthy model (left) and of the cage only model with upper disc healthy (right), when subjected to Flex.

As with E, the degenerated discs in Flex were subjected to a smaller tensile stress. The region of highest compressive stress surrounding the NP disappeared for the degenerated model, but overall the compressive stress increased in the anterior half of the disc, as depicted in Figure 5.3. The tensile stress decreased for all the constructs, from 63% in the left unilateral model to 71% in the bilateral one. The compressive maximum had a small decrease for cage only and unilateral right, a 9% increase for left unilateral and a 31% increase for bilateral.

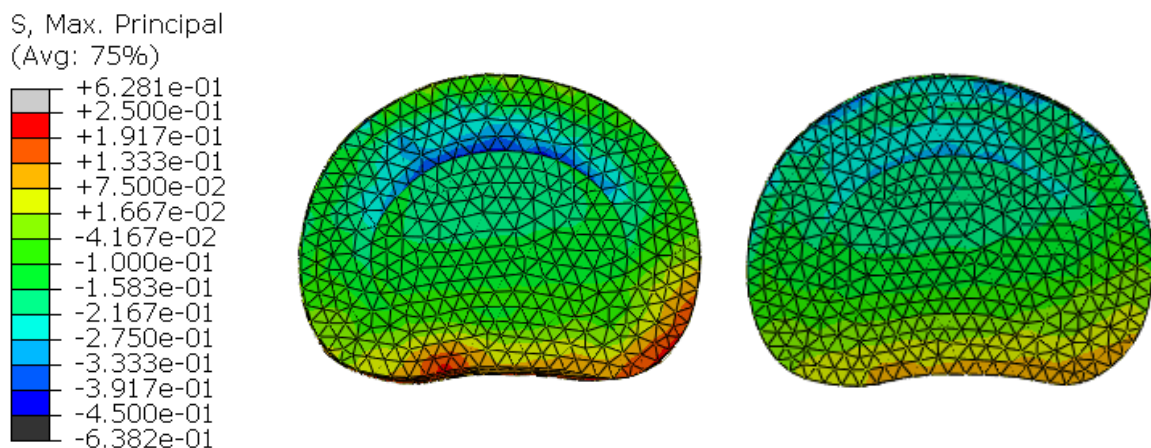


Figure 5.3 Maximum principal stress in the L3-L4 healthy (left) and mildly degenerated (right) disc when the bilateral model is subjected to Flex.

For AR the instrumented models had similar stress profiles to that of the non-instrumented healthy one. As the spine rotated to the left, a high tensile stress area appeared on the right side of the AF and the posterior parts of the AF and NP were under compression. The maximum tensile stress decreased for all the instrumented models by small percentage changes.

When rotating to the side of the instrumentation, the two unilateral models displayed similar results, however, when rotating to the opposite side of instrumentation, the unilateral right model produced a 9% reduction of the maximum tensile stress, whereas the unilateral left caused a 17% decrease. The maximum compressive stress increased 19-23% for all except the unilateral left. In this case as well, the two unilateral models behaved differently when rotating to the side opposite of instrumentation, since the unilateral left produced a 5% decrease, while the unilateral right caused a 23% increase.

AR was the movement for which there was the biggest difference between the stress profiles of the instrumented and degenerated instrumented models. As can be seen in Figure 5.4, the degenerated one didn't show regions of high tensile stress. Additionally, while the healthy disc had the anterior NP under high compression, the degenerated NP was almost all under compression with magnitude below 0.1 MPa. Although most of the posterior AF was under compression in the healthy model, the degenerated one was under tension, except for the outer rim, where a high compressive stress zone appeared. The maximum tensile stress decreased 41-45 % for all the models with degeneration, whereas the compressive stress increased.

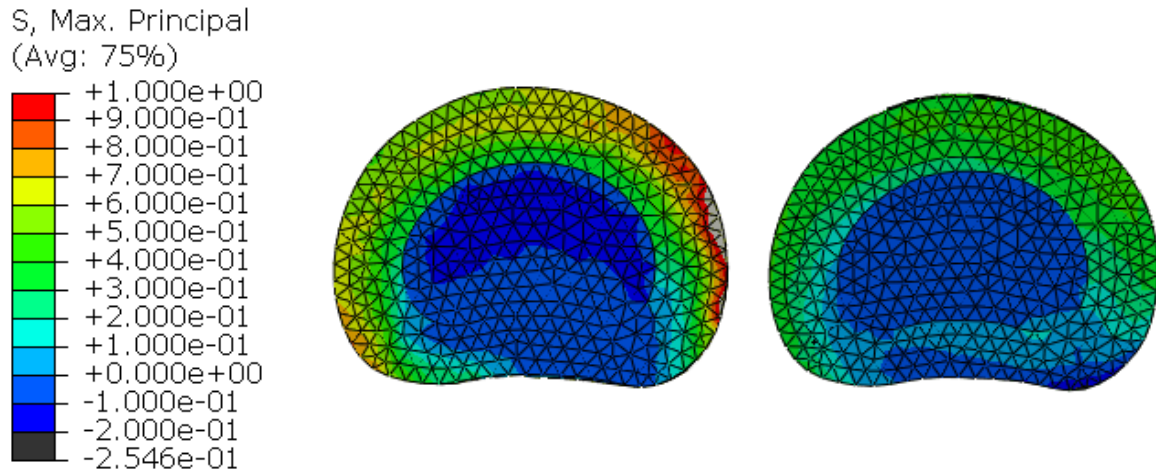


Figure 5.4 Maximum principal stress in the L3-L4 healthy (left) and mildly degenerated (right) disc when the bilateral model is subjected to left AR.

When bending to the left, the tensile stress on the opposite side of the disc was higher than when bending to the right, as can be seen in Figure 5.5 for the unilateral left model. The same was true for the unilateral right model. The maximum tensile stress decreased for all the instrumented models compared with the non-instrumented healthy one, with the cage only model presenting the biggest decrease. When bending to the opposite side of instrumentation, the unilateral left model had a 13% change, while the unilateral right one was altered by 45%. On the contrary, when bending to the same side of instrumentation, the unilateral left had the biggest change (33% versus 28% for the unilateral right one). The maximum compressive stress increased for all, except for the unilateral left model when bending to the left.

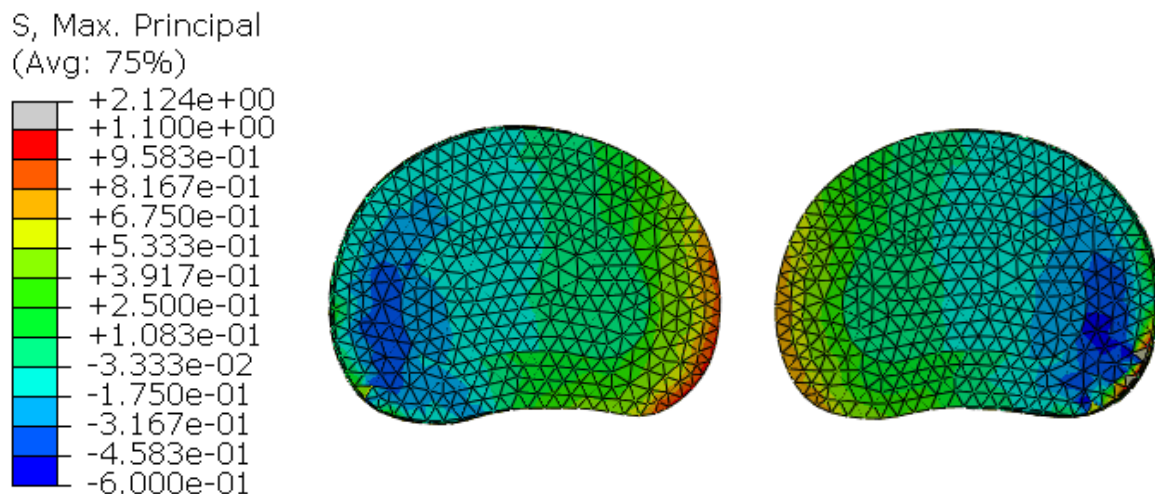


Figure 5.5 Maximum principal stress on the L3-L4 disc of the unilateral left model, when subjected to left LB (left) and right LB (right).

The biggest change with degeneration was the increase in the area under high compression, as shown in Figure 5.6. The maximum tensile stress decreased for all the constructs, from 51% for right unilateral to the opposite side of instrumentation, to 72% for left unilateral also bending to the opposite side. Upon bending to the side of instrumentation, the unilateral right had the greatest reduction (67% versus 58%). All the degenerated models had higher maximum compressive stresses than the healthy ones. This change was especially big for the unilateral left under left LB (40%) and the cage only model (27%).

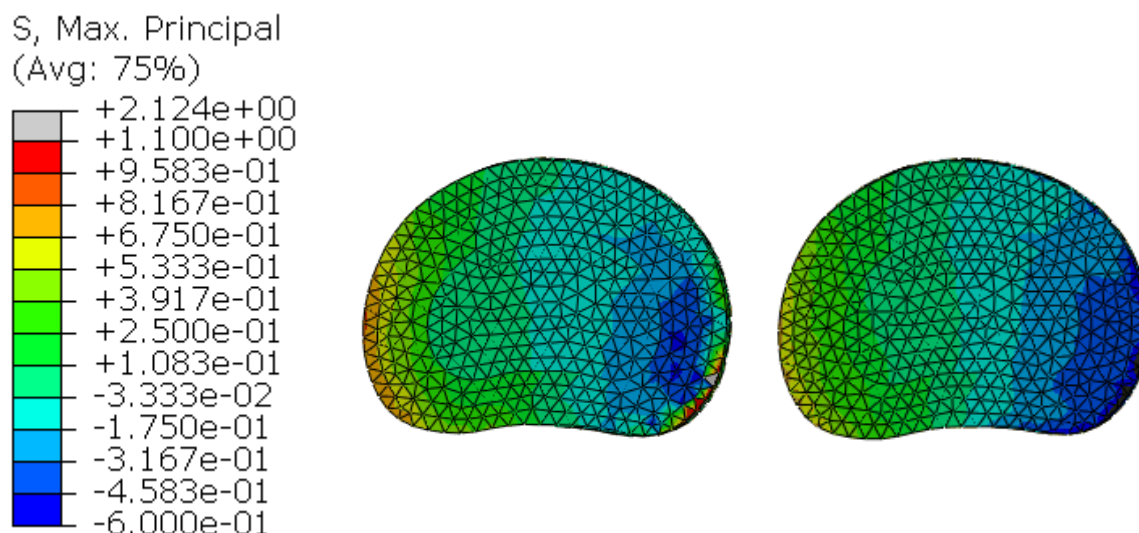


Figure 5.6 Maximum principal stress in the L3-L4 healthy (left) and mildly degenerated (right) disc when the bilateral model is subjected to right LB.

Considering just the NP of the upper level, the maximum pressure for the non-instrumented healthy, instrumented with adjacent disc healthy and instrumented with adjacent disc mildly degenerated models were compared, as presented in Table 5.13. The instrumented model showed pressures around 17% higher than the non-instrumented healthy case, in all movements except LB. When analyzing the degenerated disc, with the exception of AR, which had a 31% pressure decrease, the NP was subjected to higher pressure, with E presenting the highest percentage difference (around 48%).

Table 5.13 Maximum pressure acting on the NP, in MPa, for the non-instrumented healthy model and instrumented with bilateral fixation having an adjacent disc healthy or mildly degenerated. The values in gray are the percentage changes relative to the first case.

Movement	Healthy (MPa)	Instrumented (MPa)	P.C. (%)	Degenerated instrumented (MPa)	P.C. (%)
E	0.079	0.10	16.5	0.12	48.1
Flex	0.224	0.26	16.5	0.29	28.5
Left AR	0.202	0.24	17.8	0.14	-30.7
Right LB	0.321	0.32	0.1	0.37	14.8

Examining the stress profiles of the adjacent disc, there were no great differences among fixation types, but there were changes in the stress distribution and values from the healthy instrumented models to the degenerated instrumented ones. For E, the degenerated disc was subjected to lower tensile stress than the healthy one. Similarly, in Flex, although the healthy instrumented model had an increase in maximum tensile stress (compared to intact), the degenerated model had a lower value. Additionally, the compressive stress increased in the anterior half of the disc. AR showed the biggest discrepancy between the stress profiles of the healthy and the mildly degenerated discs: the degenerated ones didn't show regions under high tensile stress and the NP was subjected to lower compression. When undergoing LB, the area under high compression increased.

The maximum tensile stress was highest in the case of LB and smallest for E. The maximum compressive stress was highest for LB and Flex and lowest for AR.

In E, the instrumented models showed an increase in both the tensile and compressive maximums when compared to those of the non-instrumented healthy model. The same happened in Flex, except for the unilateral left and bilateral models. Also, with the exception of those two cases, both in E and Flex the maximums decreased when comparing the instrumented degenerated models with the instrumented healthy ones. From non-instrumented to instrumented and further to degenerated instrumented, LB and AR caused a decrease of the tensile maximum and an increase of the compressive maximum, in almost all the cases.

Chen et al. [7] evaluated the stress on the L3-L4 disc after ALIF at the L4-L5 level, for an L1-S1 model. They found out that, compared to the state prior to fusion, after the intervention, the stress on the adjacent disc increased for all movements (around 3.5% and 9.5% for E and Flex, respectively, and 10% for AR and LB). The percentage changes mentioned were all smaller than the ones in the present study. Since the literature model comprises the whole lumbar spine and S1, the load transmission path will be different from that of this study, considering that the adjacent lower disc will also have an increase in stress, whereas here only the upper disc will adjust for the change in behavior of the fused level.

Comparing the maximum values and calculating percentage changes between them may be misleading since there can be isolated elements with very high values of stress that are not representative of the disc as a whole. Furthermore, the non-symmetry of the model, although not important in terms of the ROM, induced differences in the way the unilateral constructs behave. Therefore, in some cases, there was not a trend in the values from the least restrictive instrumentation, the cage only model, to the most restrictive one, the bilateral model.

As mentioned in the previous section, in [47] the formulation for the most severe case of degeneration was similar to the mild state in the present study. For all movements, the authors found an increase in the pressure the NP was subjected to after PLIF, compared to the intact case. This increase was especially noticeable in E (around 33%), while for the rest of the motions it was under 6%. With degeneration the pressure further increased, particularly for AR and E. In the present work, E, Flex and AR had a similar maximum pressure increase (around 17%), while there was no variation for LB. With degeneration, LB showed the smallest change, whereas E and Flex had a considerable increase, greater than in the literature. However, AR was the only movement that suffered a decrease compared to the intact, in accordance to what happened to the maximum principal stress of the whole disc.

With the exception of AR, the results show that the NP is put under higher equivalent pressure stress after the intervention and further still with degeneration of the adjacent segment. Although there is no guarantee that this is a negative modification, the redistribution of stress by the segments adjacent to fusion has been associated with the degeneration of the adjacent discs [7].

### 5.2.2 Instrumentation

Posterior fixation reduced the Von Mises stress acting on the cage when it was subjected to the various movements. As per Table 5.14, the reduction was especially important in E, for which the maximum stress decreased around 35% for the unilateral left model and 59% for the bilateral model when compared with the values obtained for the cage only one. As expected, the reduction caused by the bilateral instrumentation was greater than that of the unilateral constructs for all the movements.

Table 5.14 Maximum Von Mises stress, in MPa, acting on the cage for the various instrumented models. The values in gray are the percentage changes relative to the cage only model.

Movement	Cage only (MPa)	Unilat. Left (MPa)	P.C. (%)	Unilat. Right (MPa)	P.C. (%)	Bilateral (MPa)	P.C. (%)
E	8.71	5.67	-34.9	5.00	-42.6	3.59	-58.8
Flex	9.397	8.15	-13.3	6.95	-26.0	6.71	-28.6
Left AR	5.156	4.57	-11.4	4.75	-7.9	3.84	-25.5
Right LB	7.523	7.13	-5.3	7.68	2.1	5.33	-29.2

Considering the comparison of the two unilateral models in AR and LB is done when both are rotating/bending to the same side or to the opposite side of instrumentation, the unilateral right showed smaller maximum Von Mises stress in all movements except Flex, as can be seen in Table 5.15. The difference between the two was more substantial when bending to the opposite side of fixation and in E (23% and 15%, respectively, relative to the values of the unilateral left).

The bilateral model showed smaller maximum Von Mises stress on the screws and rod of each side than the unilateral model of the correspondent side. Once again, the biggest differences were seen for Flex.

Table 5.15 Maximum Von Mises stress, in MPa, on the posterior instrumentation for all the types of constructs.

Movement	Unilat. Left	Unilat. Right	Bilateral	
			Left	Right
E	41.79	35.62	40.03	28.26
Flex	38.75	42.45	28.17	32.13
Left AR	28.78	33.57	24.59	31.06
Right LB	38.84	22.7	32.34	18.08
Right AR	34.64	26.51		
Left LB	23.48	29.99		

Table 5.16 presents the maximum Von Mises stress on the posterior instrumentation, for the case of a mildly degenerated upper adjacent disc. There were no great differences between the values obtained for the two degeneration stages of the upper disc, with a highest percentage difference of around 4.3% in right LB for the unilateral left model.

Table 5.16 Maximum Von Mises stress, in MPa, on the posterior instrumentation for all the types of constructs with the adjacent disc mildly degenerated.

Movement	Unilateral left	Unilateral Right	Bilateral	
			Left	Right
E	41.23	35.54	39.61	27.77
Flex	38.99	42.68	28.36	32.22
Left AR	29.52	34.79	24.56	32.11
Right LB	37.16	22.63	30.97	18.02
Right AR	35.82	26.22		
Left LB	23.34	29.02		

In the present work, bilateral fixation achieved a stronger reduction of the Von Mises stress acting on the cage than unilateral fixation. In [5] the authors simulated TLIF with a diagonal PEEK cage inserted on the bottom level of an L3-L5 model. Comparing the stress it was subjected to when considering the two types of fixation, they concluded that the unilateral case showed stresses 1.9 to 3.5 higher before fusion, whereas after fusion was achieved the ratio decreased to 0.9 to 1.2. Although the difference was more important in the literature, both works proved that the additional posterior fixation caused a cage unloading to some extent.

As for the posterior fixation, [5] displayed higher maximum stress in the unilateral screws and rods than the bilateral ones. As with the stress acting on the cage, they witnessed a bigger difference between fixation options when fusion had not yet been achieved and the interaction was simulated with a sliding algorithm and a friction coefficient of 0.2, than when fusion was implemented through a tie constraint. In the present study, only the latter interaction was tested.

Ambati et al. [46] developed an L3-L5 model, simulated fusion at the bottom segment and measured the stress on the posterior instrumentation. They found that the stress on the left unilateral screws was higher than that of the bilateral (2.7 to 6.3 times in Flex, 1.2 to 1.7 times in E, 2 to 4.1 times in left LB and 1.4 to 2.4 in right LB, while there were no big differences in AR). Although in the present study the unilateral fixation showed higher maximum Von Mises stress as well (except for the unilateral left in left LB and the unilateral right in right AR), the differences between the two types of fixation were not as marked as in the literature. It is worth mentioning that in [46] the procedure simulated was TLIF and thus all the cages were different from the one used in the present study, and so impact the posterior fixation differently.

The differences between the Von Mises stress seen for the two unilateral models, and between that of the unilateral and the corresponding side of the bilateral model were due to the asymmetry mentioned before.

All the maximum Von Mises stresses on the posterior fixation devices, both with the adjacent disc healthy and mildly degenerated, were really small compared to the ultimate tensile stress of the titanium alloy considered (around 900 MPa [37]), so the values found in the instrumentation don't pose a risk for failure and both types of fixation can be considered safe in that regard. Similarly, the stress values for the cage were small compared to the ultimate tensile stress of PEEK (90-100 MPa [36]).

### 5.3 Discussion Summary

As more serious cases of degeneration were contemplated, considering the total ROM, the spine became less mobile for E, Flex and LB and more mobile for AR. Examining only the upper adjacent level, the ROM decreased for AR and increased for the others, but all the percentage changes were rather small. On the contrary, the degenerated level (L4-L5) had its ROM intensified for AR and reduced for the other motions. According to these results, the spine became less stable for AR and had its movement more restricted for the remaining motions as degeneration progressed.

Being a two-segment model, and not one of the whole lumbar spine, as [7], the current model had bigger percentage decreases of the ROM than the literature, when comparing the cage only model to the intact one. As predicted, bilateral fixation caused the strongest ROM reduction among the constructs, followed by the unilateral model. The motion was greatly reduced at the fused level, with percentage decreases from 79.7 to 96.1%, as expected for a fusion procedure. Additionally, when comparing the ROM of the bilateral model to that of the unilateral ones, the first proved to be smaller almost 30% in E and around 20% in Flex and LB, showing that the most restrictive construct granted more stability to the motion segment. As for the adjacent segment, the greatest percentage change after the intervention was only 11%.

When comparing the instrumented constructs with adjacent disc mildly degenerated to the ones with the adjacent disc healthy, there was a ROM decrease of 10% in Flex, an increase of 57% in AR, and no changes in E and LB. When undergoing AR, the spine became less stable in the presence of a mildly degenerated adjacent disc.

As for the maximum principal stress on the disc adjacent to the fusion level, there were no big discrepancies among fixation types, but there were differences between the intact and the instrumented models and between the instrumented and the degenerated instrumented one in the stress distribution. The degenerated discs didn't show regions under high tensile stress in E, Flex and AR. As for LB, the area under high compressive stress increased for the mild disc. Considering the upper NP alone, with the exception of AR, there was an increase in the pressure it was subjected to from the healthy to the instrumented case, and further still when the instrumentation was added to a model with upper disc mildly degenerated.

The stress acting on the cage was higher when it was supplemented with unilateral than bilateral posterior fixation. Similarly, unilateral fixation showed higher maximum Von Mises stress than the bilateral instrumentation, except for the unilateral left in left LB and the unilateral right in right AR. However, the differences in magnitude between the two types of fixation were not as marked as in the literature. Moreover, the values of stress for screws/rods and the cage in the present study were all

below the ultimate tensile stress of titanium and PEEK, respectively, and so the instrumentation is safe from failure.

## 5.4 Limitations

First of all, this model was limited in the fact that its geometry was simplified and not based on medical images. However, it is worth noticing that even in the case of the latter, there is variability from patient to patient. Additionally, the model in the present study contains only two motion segments, which will not give the whole panorama of the lumbar spine. This point is especially relevant after fusion because, in a complete lumbar spine model or even in those that have the L5-S1 level below the fusion, the restriction caused by the procedure will be compensated by both the upper and the bottom segments, whereas here there was only one adjacent level. However, less complete models have also been considered in the literature to study degeneration and the effects of instrumentation, for example, an L3-L5 model as in [46] or even a single level model as used in [7].

The interaction of the facet joints was greatly simplified, while there are past studies where the facet forces are one of the evaluated parameters. The cartilaginous endplates were also overlooked in this work, whereas in others they are given distinct material properties [38].

The behavior of the IVD was made simpler in this study, while past works have mimicked swelling caused by the osmotic potential and cyclic conditions of day and rest loads [33]. This type of approach allows one to infer the intradiscal pressure, which was not possible in the present study.

In the simulation of degeneration, only the material parameters of the disc were altered, while in the literature there are more comprehensive approaches that change the disc height, the ligament properties and the size of the NP relative to the AF [38].

The cage had a simpler design than in reality. Not only did it have its upper and bottom surfaces parallel (neglecting the lordotic angle to facilitate its insertion between the vertebrae of the model), but the teeth on its surface were not represented, having been considered that the whole cage surface was in contact with the bone. Moreover, the interaction at the bone-cage interface was set as a *Tie* constraint to mimic the post-integration stage and so no comparison can be made between the behavior before and after osteointegration as in [5], for example.

# ***Chapter 6***

## **Conclusions and Future Work**

According to the results achieved in this study, the spine became more unstable as degeneration progressed, for the case of AR. For the cage only model, this was also the only movement that had a greater ROM when the cage was implanted adjacent to a mildly degenerated disc than a healthy one, which might increase degeneration in the case of an already degraded upper IVD.

Bilateral posterior fixation caused a greater reduction in ROM than the unilateral fixation, which in turn reduced the ROM more than the cage only model. Following the reasoning that a near-immobile segment is preferred for achieving adequate fusion, the bilateral posterior fixation should be the most satisfactory one.

In terms of stress, there were no major discrepancies among fixation types when comparing the stress profiles. However, there were some differences when contrasting the stress profiles of the adjacent disc when it is healthy and when it is mildly degenerated. The pressure on the upper NP increased from the healthy model to the instrumented one and further to the degenerated instrumented model. Thus, the instrumentation caused an increase in the stress which may cause degeneration of the adjacent segment. This should be taken into consideration, especially when the adjacent segment already presents suggestions of degeneration, as it might be aggravated.

As for the Von Mises stress in the instrumentation, it was higher in the unilateral fixation case, as expected since the stress is not distributed as in the bilateral construct. However, the stress values in the two fixation types were under the ultimate tensile stress for both titanium and PEEK.

As described in the Limitations section of the Results and Discussion chapter, there are numerous aspects of spine anatomy that can be added to the model or better represented in order to achieve more accurate results. It would also be interesting to see the same tests as described here performed on a model based on medical images, as the one constructed in the present work is only a simplified representation of the lumbar spine. Lastly, whereas this work took a broader approach to this subject, in the future the model could be altered to replicate specific diseases or conditions.

In conclusion, the bilateral model achieved better performance when it came to attaining fusion. However, more in-depth studies should be undertaken in order to assess whether the situation created

by either the unilateral model or the cage only one are enough to provide the necessary conditions for bone fusion. Considering stress, the results were inconclusive to decide on the type of instrumentation that would be more advantageous, as well as whether one of the unilateral models is preferable over the other. More detailed models are needed to understand the effects on the adjacent disc since in the present work it was more loaded after instrumentation, which may lead to degeneration.

# References

- [1] V. M. Ravindra *et al.*, “Degenerative Lumbar Spine Disease: Estimating Global Incidence and Worldwide Volume,” *Glob. Spine J.*, vol. 8, pp. 784–794, 2018.
- [2] B. Weisse, A. K. Aiyangar, C. Affolter, R. Gander, G. P. Terrasi, and H. Ploeg, “Determination of the translational and rotational stiffnesses of an L4-L5 functional spinal unit using a specimen-specific finite element model,” *J. Mech. Behav. Biomed. Mater.*, vol. 13, pp. 45–61, 2012.
- [3] S. H. Chen, S. C. Lin, W. C. Tsai, C. W. Wang, and S. H. Chao, “Biomechanical comparison of unilateral and bilateral pedicle screws fixation for transforaminal lumbar interbody fusion after decompressive surgery - A finite element analysis,” *BMC Musculoskelet. Disord.*, vol. 13, 2012.
- [4] K. S. Suk, H. M. Lee, N. H. Kim, and J. W. Ha, “Unilateral versus bilateral pedicle screw fixation in lumbar spinal fusion,” *Spine.*, vol. 25, pp. 1843–1847, 2000.
- [5] J. Li, W. Wang, R. Zuo, and Y. Zhou, “Biomechanical Stability Before and After Graft Fusion with Unilateral and Bilateral Pedicle Screw Fixation: Finite Element Study,” *World Neurosurg.*, vol. 123, pp. 228–234, 2019.
- [6] H. Liu *et al.*, “Unilateral versus bilateral pedicle screw fixation with posterior lumbar interbody fusion for lumbar degenerative diseases: a meta-analysis,” *Medicine.*, 2017.
- [7] C. S. Chen, C. K. Cheng, C. L. Liu, and W. H. Lo, “Stress analysis of the disc adjacent to interbody fusion in lumbar spine,” *Med. Eng. Phys.*, vol. 23, pp. 485–493, 2001.
- [8] R. Guerreiro, “Biomechanical effects of different lumbar fusion cage designs,” 2018.
- [9] Medtronic, “Oblique Lateral Interbody Fusion For L2 to L5 Surgical Technique.”
- [10] G. J. Tortora and B. Derrickson, *Introduction to the Human Body*, 9th ed. John Wiley and Sons, Inc., 2012.
- [11] H. Gray, *Anatomy of the Human Body*. 1960.
- [12] P. P. Raj, “Intervertebral disc: anatomy-physiology-pathophysiology-treatment,” *Pain Pract.*, vol. 8, pp. 18–44, 2008.
- [13] N. A. Ebraheim, A. Hassan, M. Lee, and R. Xu, “Functional anatomy of the lumbar spine,” *Semin. Pain Med.*, vol. 2, no. 3, pp. 131–137, 2004.
- [14] C. Schizas, G. Kulik, and V. Kosmopoulos, “Disc degeneration: current surgical options,” *Eur. Cells Mater.*, vol. 20, pp. 306–315, 2010.
- [15] L. La Barbera *et al.*, “Biomechanical advantages of supplemental accessory and satellite rods with and without interbody cages implantation for the stabilization of pedicle subtraction osteotomy,” *Eur. Spine J.*, vol. 27, pp. 2357–2366, 2018.
- [16] T. Lu and Y. Lu, “Comparison of Biomechanical Performance Among Posterolateral Fusion and Transforaminal, Extreme, and Oblique Lumbar Interbody Fusion: A Finite Element Analysis,” *World Neurosurg.*, pp. 1–10, 2019.
- [17] R. J. Mobbs, K. Phan, G. Malham, K. Seex, and P. J. Rao, “Lumbar interbody fusion: techniques, indications and comparison of interbody fusion options including PLIF, TLIF, MI-TLIF, OLIF/ATP, LLIF and ALIF,” *J. spine Surg.*, vol. 1, pp. 2–18, 2015.
- [18] T. Steffen, A. Tsantrizos, I. Fruth, and M. Aebi, “Cages: designs and concepts,” *Eur. Spine J.*, vol. 9, pp. 89–94, 2000.

- [19] K. Phan and R. J. Mobbs, "Evolution of Design of Interbody Cages for Anterior Lumbar Interbody Fusion," *Orthop. Surg.*, pp. 270–277, 2016.
- [20] L. C. Espinha, P. R. Fernandes, and J. Folgado, "Computational analysis of bone remodeling during an anterior cervical fusion," *J. Biomech.*, vol. 43, pp. 2875–2880, 2010.
- [21] A. S. Hilibrand and M. Robbins, "Adjacent segment degeneration and adjacent segment disease: The consequences of spinal fusion?," *Spine J.*, vol. 4, pp. 190–194, 2004.
- [22] A. H. Khalifa, T. Stübig, O. Meier, and C. W. Müller, "Dynamic stabilization for degenerative diseases in the lumbar spine: 2 years results," *Orthop. Rev.*, vol. 10, pp. 26–31, 2018.
- [23] A. J. Talia, M. L. Wong, H. C. Lau, and A. H. Kaye, "Comparison of the different surgical approaches for lumbar interbody fusion," *J. Clin. Neurosci.*, vol. 22, pp. 243–251, 2015.
- [24] S. Lu *et al.*, "An 11-year minimum follow-up of the Charite III lumbar disc replacement for the treatment of symptomatic degenerative disc disease," *Eur. Spine J.*, pp. 2056–2064, 2015.
- [25] K. Pettine, R. Ryu, and F. Techy, "Why Lumbar Artificial Disk Replacements (LADR) Fail," *Clin. Spine Surg.*, 2017.
- [26] T. Okenoglu *et al.*, "Pedicle screw-based posterior dynamic stabilisation of the lumbar spine: in vitro cadaver investigation and a finite element study," *Computer Methods in Biomechanics and Biomedical Engineering*, vol. 18, pp. 1252–1261, 2015.
- [27] D. Grob, A. Benini, A. Junge, and A. . Mannion, "Clinical experience with the Dynesys semirigid fixation system for the lumbar spine: surgical and patient-oriented outcome in 50 cases after an average of 2 years," *Spine.*, vol. 30, pp. 324–331, 2005.
- [28] T. Belytschko, R. F. Kulak, and A. B. Schultz, "Finite Element Stress Analysis of an Intervertebral Disc," *J. Biomech.*, 1974.
- [29] C. Breau, A. Shirazi-Adl, and J. de Guise, "Reconstruction of a human ligamentous lumbar spine using CT images - A three-dimensional finite element mesh generation," *Ann. Biomed. Eng.*, vol. 19, pp. 291–302, 1991.
- [30] A. M. Ellingson, M. N. Shaw, H. Giambini, and K. N. An, "Comparative role of disc degeneration and ligament failure on functional mechanics of the lumbar spine," *Comput. Methods Biomech. Biomed. Engin.*, vol. 19, pp. 1009–1018, 2015.
- [31] D. Robinson, "L3 Lumbar Vertebra," 2018. [Online]. Available: <https://grabcad.com/library/l3-lumbar-vertebra-1>. [Accessed: 28-Feb-2019].
- [32] R. Eberlein, G. A. Holzapfel, and C. A. J. Schulze-bauer, "An Anisotropic Model for Annulus Tissue and Enhanced Finite Element Analyses of Intact Lumbar Disc Bodies," *Comput. Methods Biomech. Biomed. Engin.*, vol. 4, pp. 209–229, 2001.
- [33] A. P. Castro, W. Wilson, J. . Huyghe, K. Ito, and J. L. Alves, "Intervertebral disc creep behavior assessment through an open source finite element solver," *J. Biomech.*, vol. 47, pp. 297–301, 2014.
- [34] S. Naserkhaki, J. L. Jaremko, and M. El-Rich, "Effects of inter-individual lumbar spine geometry variation on load-sharing: Geometrically personalized Finite Element study," *J. Biomech.*, vol. 49, pp. 2909–2917, 2016.
- [35] S. Naserkhaki, N. Arjmand, A. Shirazi-Adl, F. Farahmand, and M. El-Rich, "Effects of eight different ligament property datasets on biomechanics of a lumbar L4-L5 finite element model," *J. Biomech.*, vol. 70, pp. 33–42, 2018.
- [36] J. Cegoñino, A. Calvo-Echenique, and A. Pérez-Del Palomar, "Influence of different fusion techniques in lumbar spine over the adjacent segments: A 3D finite element study," *J. Orthop. Res.*, vol. 33, pp. 993–1000, 2015.
- [37] L. Klein, "TITAN Grade Nb TiAl6Nb7."
- [38] L. M. Ruberté, R. N. Natarajan, and G. B. Andersson, "Influence of single-level lumbar

- degenerative disc disease on the behavior of the adjacent segments-A finite element model study," *J. Biomech.*, vol. 42, pp. 341–348, 2009.
- [39] C. Cavalcanti, H. Correia, A. Castro, and J. L. Alves, "Constitutive modelling of the annulus fibrosus: Numerical implementation and numerical analysis," *3rd Port. Bioeng. Meet. ENBENG 2013 - B. Proc.*, vol. 7, pp. 3–6, 2013.
  - [40] F. Heuer, H. Schmidt, Z. Klezl, L. Claes, and H. Wilke, "Stepwise reduction of functional spinal structures increase range of motion and change lordosis angle," *J. Biomech.*, vol. 40, pp. 271–280, 2007.
  - [41] R. Eberlein, G. A. Holzapfel, and M. Fröhlich, "Multi-segment FEA of the human lumbar spine including the heterogeneity of the annulus fibrosus," *Comput. Mech.*, vol. 34, pp. 147–163, 2004.
  - [42] A. Rohlmann, T. Zander, H. Schmidt, H. J. Wilke, and G. Bergmann, "Analysis of the influence of disc degeneration on the mechanical behaviour of a lumbar motion segment using the finite element method," *J. Biomech.*, vol. 39, pp. 2484–2490, 2006.
  - [43] C. S. Chen, C. K. Feng, C. K. Cheng, M. J. Tzeng, C. L. Liu, and W. J. Chen, "Biomechanical analysis of the disc adjacent to posterolateral fusion with laminectomy in lumbar spine," *J. Spinal Disord. Tech.*, vol. 18, pp. 58–65, 2005.
  - [44] T. Zander, A. Rohlmann, N. K. Burra, and G. Bergmann, "Effect of a posterior dynamic implant adjacent to a rigid spinal fixator," *Clin. Biomech.*, vol. 21, pp. 767–774, 2006.
  - [45] M. Krismer, C. Haid, H. Behensky, P. Kapfinger, F. Landauer, and F. Rachbauer, "Motion in Lumbar Functional Spine Units During Side Bending and Axial Rotation Moments Depending on the Degree of Degeneration," *Spine.*, vol. 25, pp. 2020–2027, 2000.
  - [46] D. V Ambati, E. K. Wright, R. A. Lehman, D. G. Kang, S. C. Wagner, and A. E. Dmitriev, "Bilateral pedicle screw fixation provides superior biomechanical stability in transforaminal lumbar interbody fusion : a finite element study," *The Spine Journal.*, 2014.
  - [47] S. Jiang and W. Li, "Biomechanical study of proximal adjacent segment degeneration after posterior lumbar interbody fusion and fixation: A finite element analysis," *J. Orthop. Surg. Res.*, vol. 14, 2019.
  - [48] Y. M. Lu, W. C. Hutton, and V. M. Gharpuray, "Can variations in intervertebral disc height affect the mechanical function of the disc?," *Spine.*, vol. 21, pp. 2208–2217, 1996.